SCOTT:

Secure COnnected Trustable Things

Summary of selected SCOTT Building Blocks for Autonomy of Devices / Energy Efficiency of WSN

Document Type	Deliverable
Document Number	D25.4
Primary Author(s)	José Luis Burón | ACCIONA
Document Version / Status	1.1 | Final
Distribution Level	PU (public)

Project Acronym	SCOTT
Project Title	Secure COnnected Trustable Things
Project Website	www.scottproject.eu
Project Coordinator	Michael Karner | VIF | michael.karner@v2c2.at
JU Grant Agreement Number	737422
Date of latest version of Annex I against which the assessment will be made	2020-03-09

SCOTT has received funding from the Electronic Component Systems for European Leadership Joint Undertaking under grant agreement No 737422. This Joint Undertaking receives support from the European Union's Horizon 2020 research and innovation programme and Austria, Spain, Finland, Ireland, Sweden, Germany, Poland, Portugal, Netherlands, Belgium, Norway.

CONTRIBUTORS

Name	Organization	Name	Organization
José Luis Burón	ACCIONA	Hans-Peter Bernhard	JKU
Willem van Driel	PhLi	Andreas Springer	JKU
Ángel Rego	TECNALIA	Raf Roovers	NXP-NL
Javier Uceda	UPM	Melina Apostolidou	NXP-NL
Juan R. Arias	UPM	Marco Steger	NXP-AT
Antonio Barrero	UPM	Leander Hörmann	LCM
Pedro Alou	UPM	Tomas Nordström	RISE

FORMAL REVIEWERS

Name	Organization	Date
Maghsoud Morshedi	EyeSaaS	2020-02-26
Rocío Gómez, Francisco Parrilla	INDRA	2020-03-10

DOCUMENT HISTORY

Revision	Date	Author / Organization	Description
0.0	2020-01-15	M.Karner/ViF	Provided common deliverable template for Technology Lines
0.1	2020-01-24	J.Buron/ACCIONA	Initial ToC
0.2	2020-01-28	W.van Driel/PhLi	Version including BB 25.G contribution
0.3	2020-02-06	A.Rego/TECNALIA	Version including BB25.C and BB25.E contributions
0.4	2020-02-07	J.Uceda/UPM	Version including BB25.D contribution
0.5	2020-02-07	A.Springer/JKU	Version including BB25.A contribution
0.6	2020-02-07	R.Roovers/NXP	Version including BB25.B contribution
0.7	2020-02-10	L.Hörmann/LCM	Version including BB25.F contribution
0.8	2020-02-11	T. Nordström/RISE	Version including BB25.H contribution
0.9	2020-02-13	J.Buron/ACCIONA	New integrated version with Executive Summary, Objectives, and Conclusions
1.0	2020-02-21	All	Version ready for external review, after refinement addressing comments in previous version
1.1	2020-03-23	All	Improvements following external formal review

TABLE OF CONTENTS

LIST OF FIGURES

LIST OF TABLES

1 EXECUTIVE SUMMARY

D25.4 is a public summary of the overall achievements, final status of the development, and contribution to use cases of the eight Building Blocks within the Technology Line of Autonomy of Devices / Energy Efficiency of WSN.

The Building Block (BB) 25.A "*Energy Efficient Security Implementation in WSNs*" has integrated security aspects into a WSN prototype for automotive test-beds based on the EPHESOS protocol, which uses Bluetooth Low Energy Physical Layer (PHY), taking into account the energy constraints of autonomous sensor nodes. The main elements implemented in the BB are the use of Advanced Encryption Standard (AES) in Counter Codebook Mode (CCM), performing key exchange in an out-of-band manner by using Near Field Communication (NFC), and a combined routing and network concept with integrated security for combating jamming attacks. The BB is a core contribution to the use case in WP 12 "*Ubiquitous Testing of Automotive Systems*".

The BB25.B *"Energy Efficient & Resource Optimized Component Concepts for WSNs"* has developed integrated circuit building blocks for an impulse radio ultra-wideband communications sub-system, focusing on the Local Oscillator (LO) signal generation sub-system, to be used for the purposes of distance bounding in secure car access system solutions. These building blocks are integrated in System on a Chip (SoC). The BB is a core contribution to the use case in WP 14 "*Secure Car Access Solution*", where UWB radios are used to defend the car access system against so-called relay station attacks.

The BB25.C "*Energy Storage for WSNs*" has developed an energy prediction algorithm, implemented in C99 compliant code, that predicts the energy income on devices operating with a minimum amount of energy, through the adjustment of the time slots used for data transmission, in order not to deplete the energy storage system (e.g. LiPo batteries, supercapacitors, etc.). Furthermore, an adapter has been implemented for using the code as an Arduino library. The BB contributes to the use case in WP 17 *"Safe freight and traffic management in intermodal logistic hubs"*, where it is used as a power management system for the energy harvester developed in BB25.E.

The BB25.D "*Energy Supply to On Track Segment*" has developed an energy harvesting system for the electronic equipment used in on-track segments, using two primary mechanical energy sources (track deformation and air displacement when trains are passing by) as well as solar energy. The BB is composed of a vibration harvester for the energy generated by track deformation, a wind harvester for the energy generated from the displaced airflow, an AC/DC converter coupled with the previous two harvesters, a PV harvester, and a power processing unit for integrating the three primary energy sources and storing energy in a battery as a backup. The BB contributes to the use case in WP 18 "*Autonomous Wireless Network for Rail Logistics and Maintenance*", where the energy harvesting system will be installed in a working railway track.

The BB25.E *"Improved Energy Harvesting"* has developed an energy harvesting device for environments with energy sources that either are non-predictable, or are steady but generating only in the range of a few millivolts/hundreds of microvolts. The Building Block integrates hardware (energy harvesting module, MCU, and radio unit) and software (433 serial communications, energy prediction algorithm from BB25.C, energy level measurement and sleep modules) components. The BB contributes to the use case in WP 17 *"Safe freight and traffic management in intermodal logistic hubs"*, where it serves as a secondary positioning system for train wagons and containers, as a backup for the main GPS-based positioning system in case that the latter runs out of battery.

The BB25.F *"In-Vehicle WSN"* has developed a concept study of security aspects in WSN applied to in-vehicle WSNs used for measuring parameters during driving tests. The concept study consists

of 4 components: a sensor node assignment concept based on out-of-band (OoB) communication, a secure communication concept, an energy efficiency concept for an energy efficient implementation of the previous two components, and an online security check concept. The BB contributes to the use case of WP12 "*Ubiquitous Testing of Automotive Systems*", where some parts such as secure key exchange via NFC and encrypted communication are implemented in the demonstration.

The BB25.G "*System Level Availability*" has investigated to what level fault injection can contribute to a faster release of large and complex systems. The technique has been demonstrated through the InterAct Office (a LED retrofit system), using an available test bed. The BB is applicable for the use cases in WP7 "*Air Quality Monitoring for Healthy Indoor Environments*" and WP12 "*Ubiquitous Testing of Automotive Systems*.

The BB25.H *"Dependable and resource-optimised wireless technologies for trustworthy WSNs"* has addressed different aspects of energy efficiency and resource optimization supporting efficient and secure network deployment, runtime operation, and maintenance of in-vehicle networks. Furthermore, the BB has developed methods for coordinating the interaction between multiple DEWI bubbles. The BB contributes to the use case in WP13 "*Trustable Wireless In-vehicle Communication Network*", as part of the demonstrator.

Keywords: energy harvesting, energy efficiency, energy storage, energy prediction, energy efficient security, track deformation, air displacement, trustworthiness, fault injection, Contiki-NG.

2 OBJECTIVES

The main goal of the Technology Line Autonomy of Devices / Energy Efficiency of WSN is the development of an advanced strategy for addressing cost-efficiently the energy requirements of wireless sensor networks designed for different applications and domains.

This strategy consists of a set of technologies and concepts supporting three main areas for the improvement of autonomy of devices and energy efficiency of WSN:

- Identification, development and integration of the most suitable energy harvesting and energy storage technologies.
- Development of energy-efficient components and communication protocols for WSNs.
- Physical/logical integration of energy-constrained sensor networks.

The Technology Line is linked to the high level objective #3 of the SCOTT project, which is to extend the Internet of Things concerning Autonomy of Devices / Energy Efficiency of WSN. The development of the Technology Line is broken down into a set of eight re-usable Building Blocks that are being integrated into several SCOTT use cases from different domains. Seven of these Building Blocks (BB25.A to BB25.G) have been defined since the beginning of the project, while the eighth Building Block (BB25.H) was added following an amendment of the project carried out in 2018.

D25.4 provides a public summary of the overall achievements and final status of the development of each Building Block and their respective contributions to the SCOTT use cases.

3 DESCRIPTION OF WORK

The development of the Technology Line is broken up into re-usable Building Blocks. Thus, WP25 has developed 8 Building Blocks, from BB25.A to BB25.H, for their application in several use cases from different application domains in SP2. The Building Blocks are described in detail in the following subsections.

3.1 Building Block BB25.A Energy Efficient Security Implementation in WSNs

The goal of the BB25.A "Energy Efficient Security Implementation in WSNs" is to enhance an existing WSN prototype for automotive test-beds, i.e. an engine test-bench, by security measures. However, because the sensor nodes of the WSN prototype should be powered by a solar cell, the tight energy budget and the low computational resources should be kept or need at least to be considered. The remainder of the section presents the description of the BB and its implementation.

3.1.1 Main Achievements of the Building Block

The WSN prototype for automotive test-beds, which existed already before the SCOTT project started, is based on the EPHESOS protocol and uses the Bluetooth Low Energy PHY. A description of EPHESOS can be found at [1]. In order to include security aspects, we followed the Spoofing, Tampering, Repudiation, Information disclosure, Denial of service, Elevation of Privilege (STRIDE) methodology. Therefore, the protocol was described in its six phases: pairing, storage, rigging, idling, measuring, unmounting. The STRIDE threat classification model enables to systematically model threats according to the six categories: (1) spoofing identity, (2) tampering with data, (3) repudiation, (4) information disclosure, (5) denial-of-service, and (6) elevation of privilege. In total, 23 threats in 8 different classes (eavesdropping, jamming and muting, tampering, spoofing and replaying, physical attacks, threats related to clock synchronization, NFC-related threats, further threats) were identified. STRIDE has been initially developed for ordinary software, i.e. on commodity hardware, in mind rather than with wireless sensor networks. Thus, the categories did not appear fully appropriate. Especially the energy budget of autonomous sensor nodes is a crucial parameter influencing the measures on security.

Based on the results of the threat analysis, we focused on (i) the use of Advanced Encryption Standard (AES) in Counter Codebook Mode (CCM) which provides symmetric encryption and which is available as a hardware module on the used chip, (ii) performing key exchange in an out-of-band manner by using NFC (see BB 23.F – Out of band security), and (iii) a combined routing and network concept with integrated security for combating jamming attacks, (equivalent to denial-of-service attacks), which also takes the energy of the nodes and timing constraints into account.

For combating jamming attacks, which are equivalent to denial-of-service attacks, we have developed BASEBAL (**BA**ckward **S**tructured **E**nergy **BA**lanced **L**ink) a combined routing and network concept with integrated security which allows for an energy efficient implementation. Moreover, constraints such as defined low latency contribute to the complexity, but also point a way to the solution of the problem. The implementation of the BASEBAL routing algorithm consists of two parts: (1) network discovery and (2) network link phase. The network is organized in layers. The nodes of layer *n* are connected to nodes of layer *n-1* and *n+1*. In layer 0 only the base station (BS) is considered. Nodes that can receive beacons transmitted from Base Station (BS) are considered to be in layer 1. Next, considering the layer 1 nodes as a relay, the beacons transmitted from the base station can now be relayed further. Thus, all nodes who receive the beacons at this stage are

considered as part of layer 2. The network discovery continues until all nodes are discovered and sorted into layers.

The implementation of the BASEBAL routing algorithm as described in [2], follows the network discovery step. All possible routes start at the base station and each route connects one node out of the total amount of nodes in the network. The algorithm starts at the last layer and navigates backwards. A visualization of the result of the routing algorithm is given in Figure 1, where green lines denote best routes, optimized by the routing algorithm, whereas gray lines denote all possible connections in the network after network discovery. The red numbers display the energy budget of the respective nodes, which is taken into account by the BASEBAL routing algorithm, e.g. all nodes with an energy budget of only 1 are not able to act as relay.

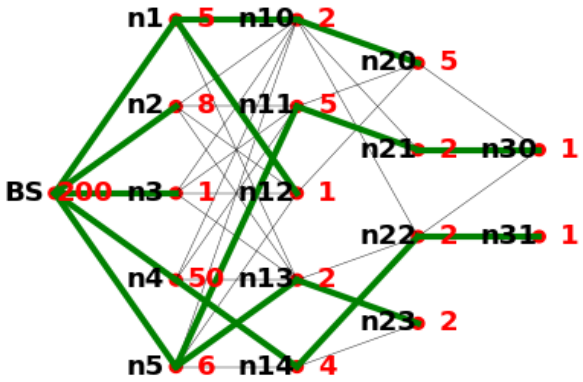

Figure 1: Result of the BASEBAL routing algorithm

Various measured parameters are planned as indicators for ongoing attacks or vulnerability. The Packet Error Rate (PER), the inter-node synchronisation and the end to end synchronization indicate whether a connection between two nodes is suspicious or not. If the location of the nodes is known, routing contributes to localize the position of the disturbance. In Figure 2 this is visualized. Here the data received by the nodes marked in red indicate that the wireless links are somehow disturbed. This allows not only for a re-routing (e.g. node 31 could send its data to N22 instead to N10) but also shows the geographic area and the direction at which the distrurbance occurs. In this example all disturbed links/nodes appear in the same direction. It is thus highly likely that all nodes are disturbed by the same kind of interference, e.g. a jammer.

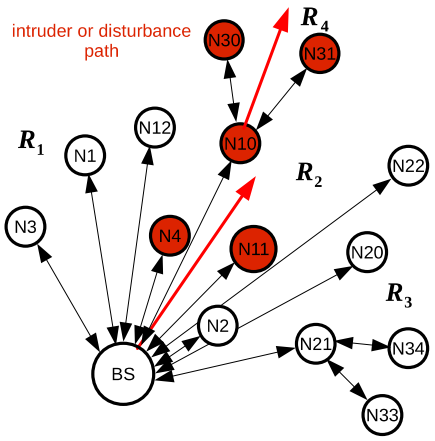

Figure 2: Setup for routing concept and intruder path detection

Due to the EPHESOS protocol, the nodes and the base station are pairwise synchronized. Each hop increases the latency by one hop delay and because the nodes are synchronized the delays are known and can be used as a measure against relay attacks. With respect to combating jamming attacks, if we consider Figure 2, it can be clearly seen that, if there is a local network disruption, a path to the malfunctioning nodes can be found. The measures to qualify a disruption are delay variations, Received Signal Strength Indicator (RSSI) changes, packet loss or similar error-indicating measurements. The routing protocol was designed with communication links to propagate this surveillance information as meta information constantly while the network operates.

The routing concept is developed with a central logic in the base station, controlling, computing, storing and communicating the routing path. All information is collected centrally and distributed as processed information in the form of a trust indicator, the routing path and the trust value of the routing path. In Figure 3, we depict the developed timing structure of the EPHESOS protocol assisting routing. In the continuous mode of EPHESOS, in which each node transmits its data on a regular basis, commands are sent throughout the network via beacons at the start of the super frame or in the time slot of an individual hop node like N1 in Figure 3. This is processed by the BASEBAL algorithm with integrated commands in the EPHESOS framework. The key exchange for encrypted communication happens in a key box prior to the routing setup. Thus the routing data and metadata exchange can be done securely according to the security concept of star topology networks.

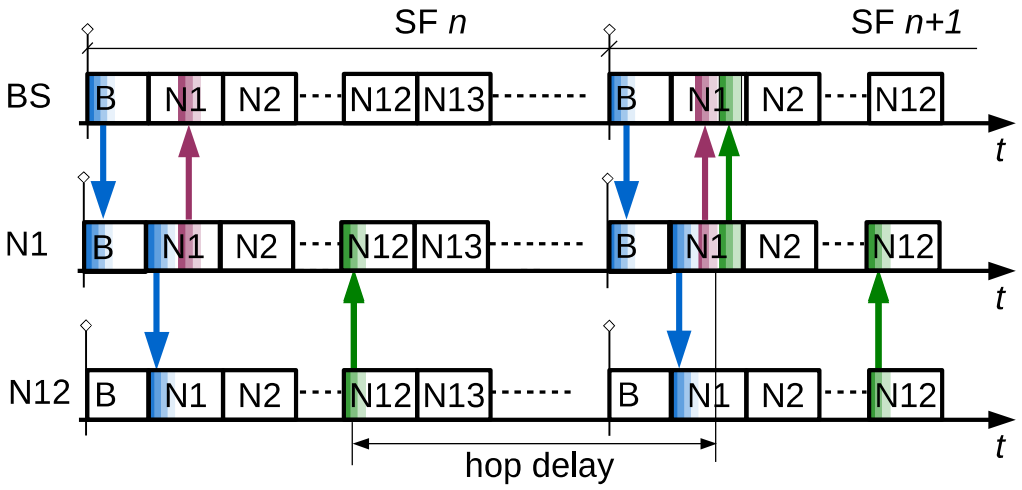

Figure 3: Timing slot organization for routing

Within SCOTT we designed a monitoring protocol via the Universal Asynchronous Receiver Transmitter (UART) of the nodes. The monitoring protocol is necessary to communicate with external hardware and software. The data are stored externally for further processing on external hardware with higher computational power for statistical evaluation. All the collected and processed data is used to create ground truth data for the classification of reliable and non-reliable links. Moreover, it will lay the base for further evaluation algorithms on the nodes or the base station to decide whether the path or link is trustworthy or not. Identifying jamming is the first step in testing the network against disruption. The jamming itself is described in D23.3 (Security Building Blocks) by Gdansk Technical University (GUT) [3]. Additionally, the protocol is used to synchronize the cameras for the optical localization system developed by GUT.

3.1.2 Final Status of the Building Block & Contribution to Use Cases

The status of the described elements of BB 25.A “Energy Efficient Security Implementation in WSNs” are as follows:

(i) The use of AES in CCM which is available as a hardware module on the used chip providing symmetric encryption is implemented.

(ii) Performing key exchange in an out-of-band manner by using NFC (see BB 23.F – Out of band security), is implemented

(iii) A combined routing and network concept with integrated security for combating jamming attacks, (equivalent to denial-of-service attacks), which also takes the energy of the nodes and timing constraints into account. A fixed latency energy efficient two hop routing network is implemented as a proof of concept.

BB 25.A is targeted to use case WP 12 "*Ubiquitous Testing of Automotive Systems*" and is a **core** contributor to WP12.

According to D12.1 "*Use Case Specification 'Ubiquitous Testing of Automotive Systems'*" [4], BB 25.A is specifically targeted to Scenario 4 "*Run tests (operate and monitor Unit Under Test (UUT), test bed/vehicle and measurement system)*" of use case WP 12 "*Ubiquitous Testing of Automotive Systems*". However, the security aspect covered in this building block – key exchange, authentication, and data encryption – are relevant to most of the scenarios of WP12.

3.2 Building Block BB25.B Energy Efficient & Resource Optimized Component Concepts for WSNs

NXP-AT and NXP-NL have committed to study and prototype integrated circuit building blocks for an impulse radio ultra-wideband communications sub-system to be used for the purposes of distance bounding in secure car access system solutions. The primary recipient of our work within SCOTT will be WP14, use case "*Secure Car Access Solution*".

NXP proposed already the communications sub-system on the physical layer defined in IEEE standard 802.15.4-2015, more specifically the High Rate Pulse (HRP) UWB physical layer. With this choice of physical layer, we expect to meet the distance bounding accuracy requirements while at the same time achieving the targeted autonomy and energy efficiency required for a battery operated system.

The impulse radio ultra-wideband distance bounding sub-system will increase the security of car access solutions in which it will provide a means to detect and effectively defend against a certain type of attacks against the current car access solutions.

3.2.1 Main Achievements of the Building Block

NXP decided to focus on the local oscillator signal generation sub-system (see Figure 4), an essential part of an integrated UWB system on chip.

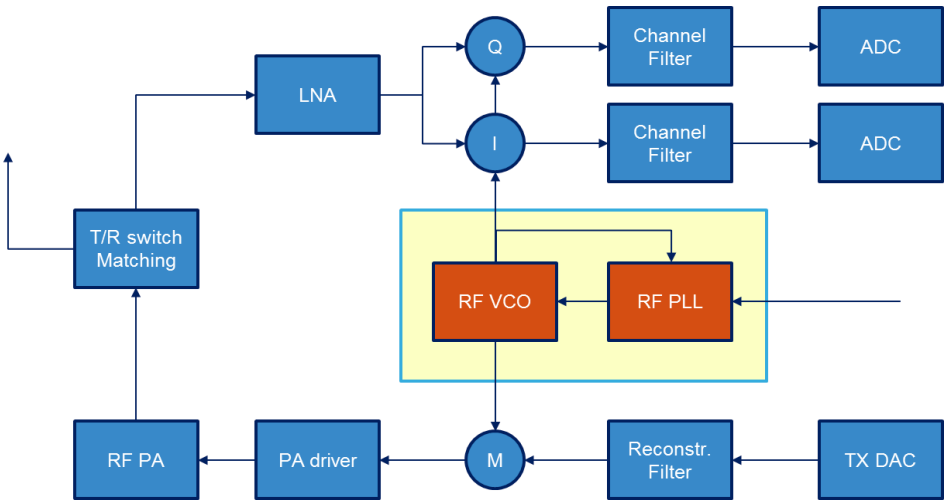

Figure 4: Block diagram radio transceiver subsystem

Figure 5 shows detailed functional sub-blocks of the timing generator for which the specifications have been derived to meet the overall tight Time-of-Flight (ToF) measurement accuracy. The building blocks are complemented with supporting power supply and biasing blocks specified to guarantee performance when integrated into SoC over temperature and supply voltage range.

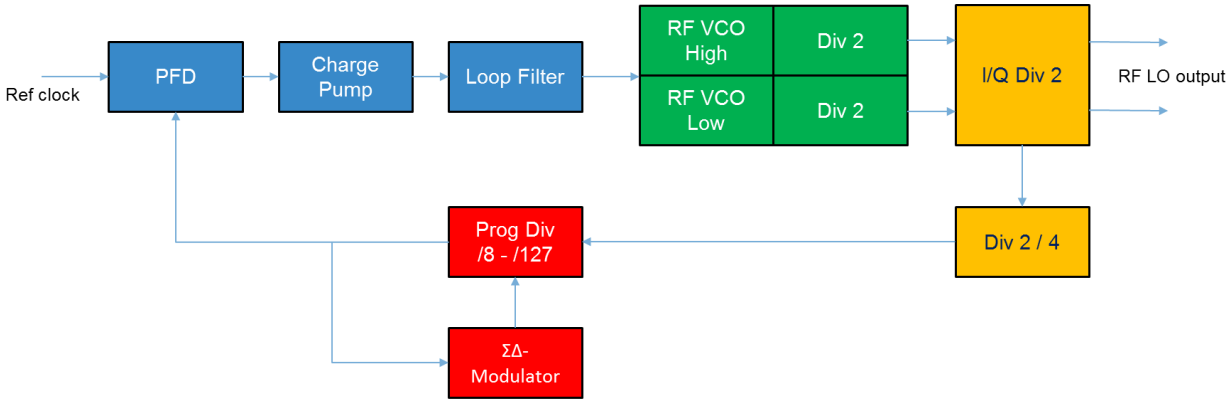

Figure 5: Building Blocks of the Local Oscillator Signal Generation

Achievements summary:

1. All building blocks designed, simulated and characterized and made up to specification for the whole temperature, voltage and process corner variation while maintaining power consumption within the target.
2. Process and temperature reference clock (crystal) compensation and trimming implemented and results are better than +/-20ppm when including ageing. Our solution complies to the IEEE standard.
3. Indirectly, via point 2, we proved that our trimming methodology with General Purpose (GP) ADC for accurate temperature measurements is effective.
4. Process and temperature Voltage Controlled Oscillator (VCO) frequency calibration, to limit further the Vtune range variation and keep phase noise performance in optimal range was confirmed during characterization. Measured Calibration time better than 100us.

5. Building blocks integrated into full SoC. On the SoC, analog, digital and software are working together for Phase-Locked Loop (PLL) frequency generation, calibration and compensation while keeping performance in place.

Building blocks tested in SoC validated under all process technology variation, voltage and temperature (PVT) conditions. Figure 7 and Figure 8 are snapshots of the UWB Tx modulated signal that complied to the IEEE standard by using the local oscillator signal generation.

Our design achieves the required performance while being state-of-the-art in power efficiency. One of the sub-blocks that can capture the performance versus power efficiency trade-off is the Voltage controlled oscillator (VCO). A well defined VCO figure-of-merit (FOM) accepted by the scientific community is

$$FOM_{VCO} = -L(\Delta\omega) + 20\log\left(\frac{\omega_0}{\Delta\omega}\right) - 10\log\left(\frac{P_{diss}}{1mW}\right)$$

where w_o is the carrier frequency, L(dw) denotes the VCO phase noise in dBc/Hz at dw offset from the carrier, and P_{diss} is the total dissipated power, both measured at w_o frequency. For the VCO design we measure a state-of-the-art FOM of 187dBc/Hz(at 32GHz) and 189dBc/Hz(at 26GHz) of operation within the highly integrated 40nm CMOS technology [8].

3.2.2 Final Status of the Building Block & Contribution to Use Cases

NXP-AT and NXP-NL have developed integrated circuit building blocks for an impulse radio ultra-wideband communications sub-system to be used for the purposes of distance bounding in secure car assess system solutions. The building blocks are integrated into SoC and are part of system demonstrator. The primary recipient of our work within SCOTT will be WP14, use case "*Secure Car Access Solution*".

A picture of the SoC on characterization board with integrated LO signal generator area is captured in Figure 6.

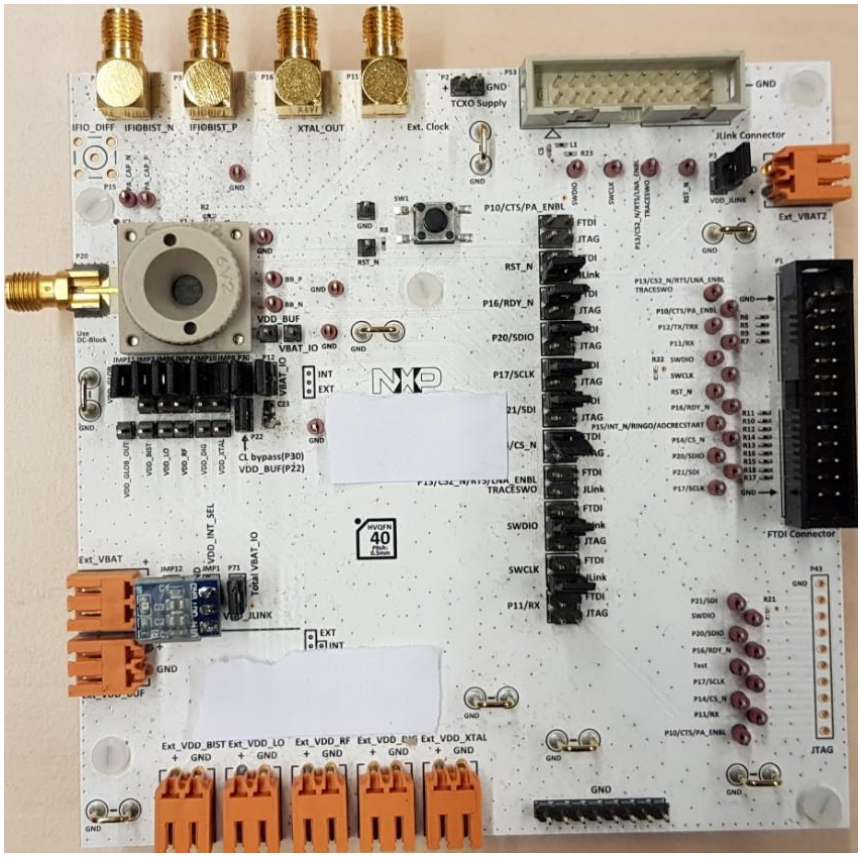

Figure 6: Characterisation test board with UWB IC

Functionality and performance of the LO signal generator within the SoC is measured for typical material, confirming the block specification and the overall system is in line with the system requirements.

Measurements on our SoC validated the IR-UWB functionality. Figure 7 and Figure 8 show time and frequency domain measurements of an UWB TX Modulated signal with 6.5GHz Carrier with 14dBm Peak Power.

In Figure 7, the graph captures the amplitude of a ranging frame which consists of the SYNC preamble, the start of frame delimiter (SFD), the secure training sequence (STS) and finally the payload.

In Figure 8, the Y-axis denotes the power spectral density of the signal dBm/MHz and x-axis marks the frequency. One can see the occupied bandwidth of the signal and the compliancy to the spectral regulations (red solid line).

Figure 7: Time-domain UWB TX Modulated signal with 6.5GHz Carrier with 14dBm Peak Power.

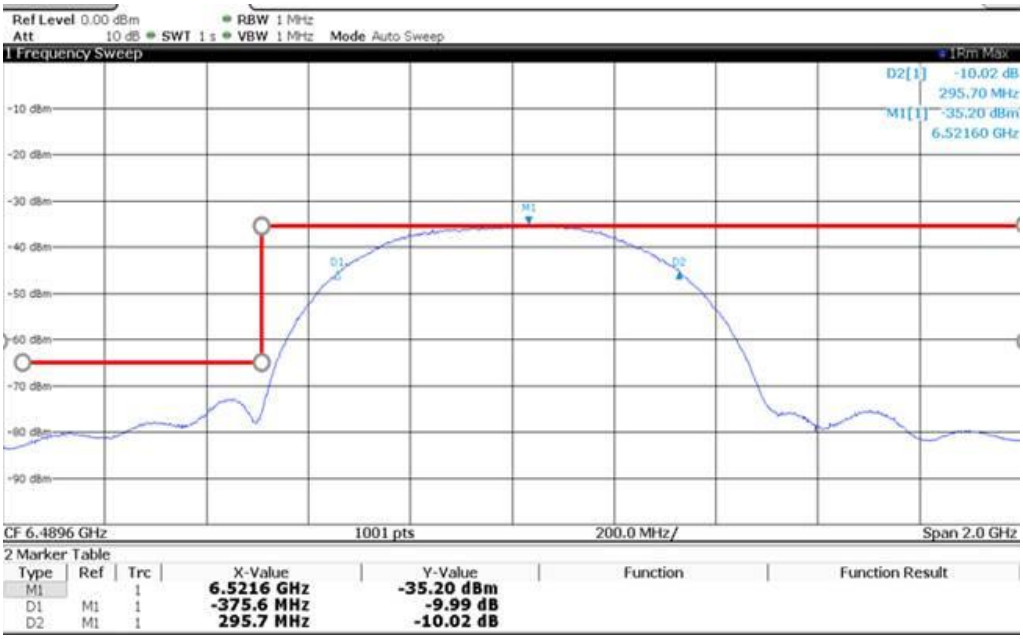

Figure 8: Frequency-domain UWB TX Modulated signal with 6.5GHz Carrier with 14dBm Peak Power.

The developed building blocks in BB25.B are meeting all requirements across process technology variation, temperature and power supply range (PVT).

The developed UWB SoC is integrated in the system demonstrator developed in WP14. A car access system typically consists of a combination of LF, for polling and distance estimation between car and key fob, and RF for remote opening functionality. The UWB radios are added to defend the car access system against so-called relay station attacks. To achieve this, WP14 employs the high-accurate, high-secure ranging ability of UWB to establish a distance bounding feature making relay station attacks practically impossible.

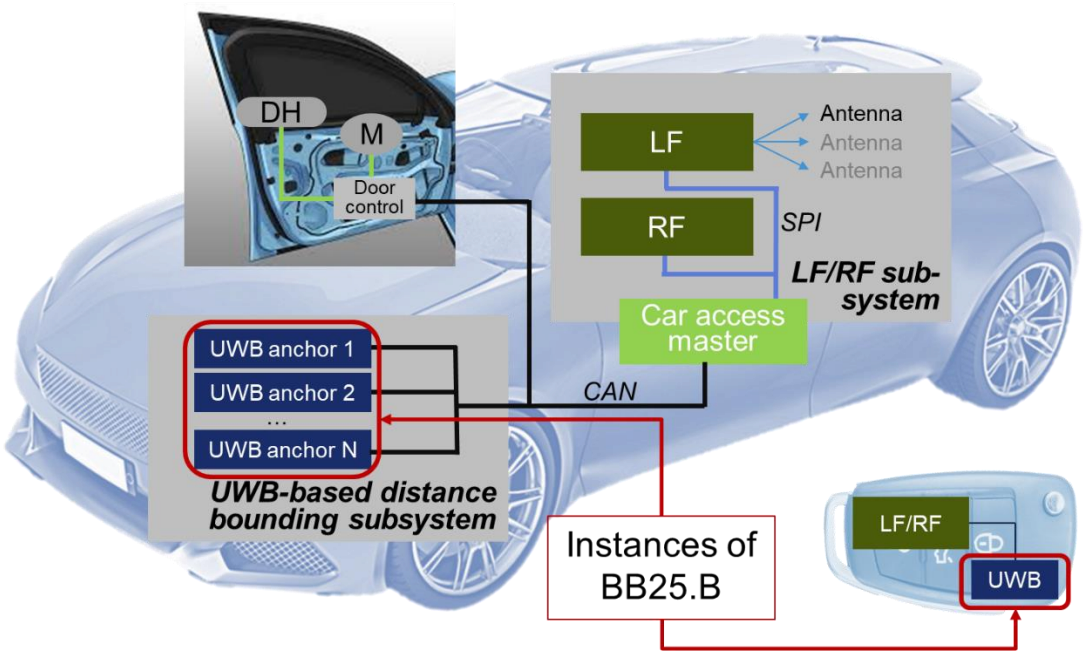

Figure 9: Usage of TBB BB25.B in SCOTT use case 14: secure car access solution

3.3 Building Block BB25.C Energy Storage for WSNs

TECNALIA has developed an Energy Prediction algorithm to predict future energy income on a device operating with a minimum amount of energy, by adjusting the time slots to transmit data without depleting its battery. This algorithm considers the energy storage limitations of the system and it crosses this information with the average harvested energy coming from different energy sources. The algorithm considers also historical collected data when possible (i.e. daily energy income is regular), as well as prediction ahead of time based on energy income of the latest slots.

3.3.1 Main Achievements of the Building Block

Energy Prediction Algorithm

The prediction algorithm is a C99 compliant code (so it can run on a wide range of Microcontroller Units – MCUs) and some adapters for different microprocessors, in this case, an adapter for using it as Arduino library has been implemented. The algorithm must be pre-configured depending on the energy storage system. LiPo batteries work at low MAX voltage and they have slow charging rates, but the minimum safe energy barrier to trigger power-save mode can also be lowered. On the other hand, supercapacitors can operate at higher MAX voltage, and the charging rate is much faster compared to batteries, but the trigger to power-save mode must be adjusted for pessimistic cases, otherwise, the energy could be depleted fast because the energy density is nowadays much worse than the existing technology for batteries.

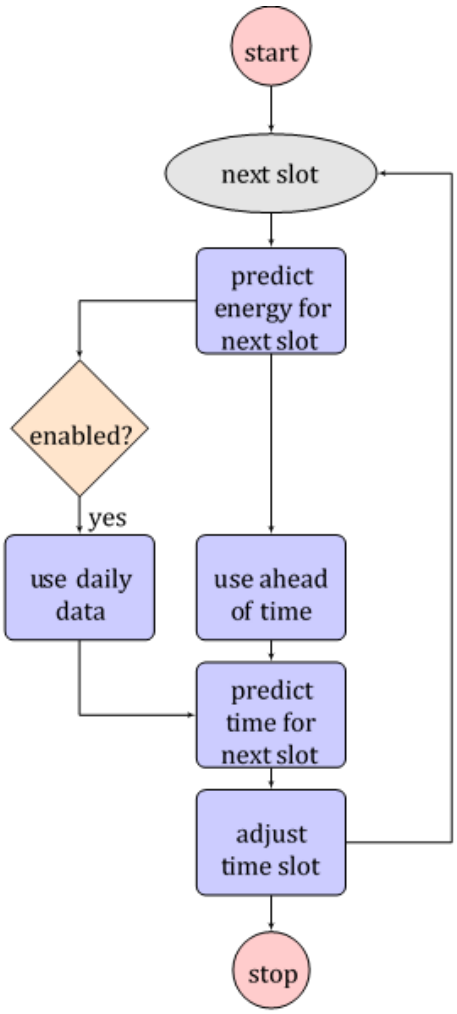

Figure 10: Energy prediction algorithm workflow

The algorithm is based on a closed loop waiting until current time equals the stored time limit. Then, the algorithm calculates the energy difference that the device will gain or lose in the next expected timeslot. Since the power sources where the device is stored can have a recurrent source (i.e.: solar) or non-recurrent (i.e.: wind drafts, vibrations, thermal changes), the energy prediction is divided into history-based and real-time based.

The history-based power prediction system has several constraints caused by the low-power energy consumption that the device is expected to use. Therefore, there is no communication to central servers to send data/retrieve decision or storing power intake/consumption historical data. By removing communication with central server to predict energy, the energy consumption is greatly reduced (please note that a radio is still attached to the harvesting device to send data when the algorithm decides that a message can be sent when energy conditions are valid). By discarding historical data storage and calculations, small and low energy storage systems can be attached to the device, and fewer microprocessor cycles are executed, so the resulting device is more inexpensive and more energy efficient.

The typical procedure to decide if the power sources are stable or recurrent is by checking power availability during a full day. Some devices are designed to operate outdoor where the solar power is the main ambient source during the day. Other devices can be recharged by using piezoelectric or electromagnetic sources caused by most of the works that are usually executed during the time humans are working (vibration from transport operations, opening/closing doors and so on). The

decision diamond box in the algorithm is intended to check if the power intake has enough predictability to be able to analyze if the energy state of the device can be calculated for the next hour because the last day, at the same time, the difference between the hour and the next hour is available, and since the source is stable during the day, the future energy status of the device can be calculated.

Even if this prediction based on historical data is useful, there are times when the availability of ambient power sources can change. For instance, the device can be re-attached to another host (truck, container, etc.) or installed in a location where the solar power is not available. For these cases, the daily based prediction branch is discarded, and the only source of truth is the energy differences between a short time period. This is the case for the ahead of time calculation of the energy. If battery power was at 50% in the last checked step, and in the current step the battery value is 55%, the system can anticipate that the energy being harvested will be more than the energy spent by the device operation.

By using the energy prediction of the current, short term prediction, and the daily based prediction (if conditions to enable it have been reached), the next block is to predict a new time slot where device can operate and send data without depleting its battery in the near future. In this case, several formulas can be set to match energy predicted in the future with the time slot that the device can send data. For instance, a logarithmic formula can foster much higher frequency of operation when battery values are high, and much lower frequency (and therefore infinite time slots) when the battery is so depleted that the device could be completely stopped. Leaner formulas to emulate the logarithmic could be used to perform fewer microprocessor cycles, but for lowest power consumption, a discrete, linear formula (as seen above) is preferred because the calculation can be performed in few cycles.

Once the total energy to be gathered has been calculated, the next step is to adjust the time slot of the device to send information via wireless. The energy cost of the leakages, algorithm and radio transmission is enough stable to compute the delta between the energy increase and the energy consumption, so the system can ensure the best dynamic period to send data without compromising battery level, even if ambient sources of energy change suddenly (from good conditions like direct solar power to bad conditions like changing the item to a shaded area).

When the new timeslot is set, the device can be sent to sleep mode. This device could be wake-up either when a voltage comparator measuring battery level trigger the action, by using a watchdog to periodically check if the time to trigger the radio transmission has been reached, or by other means, but also taking into account that the solution should spend the minimum energy consumption to operate. When the device hosting the prediction algorithm is being deployed on static places, the available ambient source of energy can be better predicted so the device could be continuously running (and the only constraint is to limit when to transmit data) but for general purpose, low power devices, setting the device to sleep mode covers a wider range of operational scenarios.

Configuration of the algorithm

The library is time-slot configurable, the default values are 1/10/100, so a normal operation would translate period by multiplying the timeslot returned by the algorithm.

The health barriers are also configurable sliders. Depending on real use cases, the healthy battery range can be from 10%-100%. For other cases where the energy intake is unpredictable, a safe range could be 50%-100%. The default barriers, in conjunction with the period multiplier are 0%-100% (even if the sliders are at 30% 60%, but values below 30% still emit once every 100 times).

Tuning the algorithm for different power sources

For LiPo batteries: typical operating voltage ranges from 3.5V to 4.2V, so the parameters in the algorithm should be E_LOW=3.7V=20% and E_HIGH=4V=80%. In these energy storage systems, the discharge rate is mostly linear so the formula could be adjusted wider (5% to 100% of predictor linear operation).

For supercapacitors: operating voltage from 1.8V or 2.7V (depending on MCU) to 5V (5.5V is limit in specs). But for the commercial 433 modules, the minimum voltage to operate is 3.5V. Therefore, the real operation voltages for the predictor is 3.5V-5V. The discharge rate for these devices is not linear ($E=1/2*C*V^2$) so the minimum barrier should be enough generous to prevent the capacitor energy to be depleted. In this case, since the lower limit is set by the radio module and it is higher than 50% capacitor, the lower limit will be safe. But for other radios, or when using a boost converter, as pre-step for the communication module, the min value would go back to 1.8V. In normal operations of the current harvester, E_LOW=3.7V and E_HIGH=4V are also good values, and compatible with the LiPo option.

The real operating voltage are 3V (current radio min to operate) minimum and 4.2 or maximum 5V.

For the LiPo version, the battery percentage and predictor barriers are (4.2-3.5=0.7):

100% 4.2V

80% 0.8*0.7+3.7=4.06V

20% 0.2*0.7+3.5=3.64V (above 3V)

0% 3.5V

For the supercapacitor option, if we keep that energy_0=0V but operation minimum is 3V (V100-V0=5-0=5):

100% 5V

90% 0.9*5+0=4.5V

70% 0.7*5+0=3.5V (above 3V)

0% 3.5V

Finally, if we use supercapacitor but set minimum to 3V, and given the fact that percentage is quadratic to the voltage $E=1/2CV^2$ (so we could assume 3V as 0% with some error) we could use the same configuration limits in code for both the battery and the supercapacitor (only change the max value) (V100-V0=5-3=2).

100% 5V

80% 0.8*2+3=4.6V

20% 0.2*2+3=3.4V (above 3V)

0% 3V

Installation as Arduino library

The library can be provided as a zip file so the Arduino library manager wizard will take care of the library.

Execution of the algorithm

There is an Arduino project to test the energy algorithm, so it is as easy as to burn the code with the default configuration. Please note that these implementations are only wrappers for MCUs, the

library itself is MCU agnostic, so the only requirement for using the algorithm is to have a C99 compliant compiler.

Note that there is a `PRODUCTION` flag in the Arduino project. This flag is only useful when testing code when plugged to the laptop USB or to a power source. The default value is `PRODUCTION=true`, this value is valid for the 90% of the cases where the code is being tested so do not change it.

Note also that `VCC_MAX` is also useful to make the different power sources to have a canonical value. The ATTYNY85 can operate from 2.7 (or 1.8V in L models) to 5.5V in general, while the internal Vref is set to 1.1V. Therefore LiPo 100% battery is adjusted to VCC_MAX=4300 mVolts while 5V supercapacitors will be adjusted to 5000 (and 2,5V supercapacitors to 2500 and so on).

After adjusting the predictor to E_MAX=5V and E_MIN=3V (adjustment for supercapacitors), the operation time of the harvester has been 12 hours sending data at different intervals without recharging.

3.3.2 Final Status of the Building Block & Contribution to Use Cases

Status

The Building Block is completed. Tests on the lab are running continuously on the current devices where the algorithm has been installed. Some refinements will be made after real deployment in use case. Costs of storage solutions are very inexpensive. The supercapacitor version as storage (and considering future improvements on general availability of supercapacitors) is good enough to cover cases where energy intake is unpredictable, but it can be gathered fast once occurred.

Contribution to Use Cases

The current Building Block is intended to be deployed in the SCOTT use case WP17 "Safe freight and traffic management in intermodal logistic hubs". The energy prediction algorithm to be developed as key power management system for low constrained devices will be installed into a device known as the “Energy harvester”, a low power, low resources, and inexpensive device that has been developed in the BB25.E. This device will act as a secondary positioning system, with weak precision compared to other solutions, but prepared to work autonomously and with no maintenance at all, once installed (see BB25.E description).

3.4 Building Block BB25.D Energy Supply to On Track Segment

The BB25.D “Energy Supply to On Track Segment” is conceived to provide harvested energy to the electronic equipment used in the on-track segment. The energy is harvested from two primary mechanical sources generated by track deformation and air displacement when a train is passing by, and a third source generated by solar photovoltaic panels. These three primary sources are integrated in a single BB, storing energy in a battery as a backup, due to the intermittent nature of the energy primary sources.

The amount of energy harvested in the BB is highly dependent on the traffic conditions and solar radiation. Practical designs need to be adapted to the particular conditions of the application scenarios and the power requirements from the loads.

3.4.1 Main Achievements of the Building Block

The main achievements in the BB25.D are described in the following sections. In Section 3.4.1.1, the harvester architecture is described. Section 3.4.1.2 is focused in the Vibration Harvester Unit. The Wind Harvester Unit is described in Section 3.4.1.3, PV Harvester in Section 3.4.1.4, and finally Storage and Power Processing Unit is described in Section 3.4.1.5.

3.4.1.1 Energy harvester Architecture

The harvester is finally composed of four units:

- Vibration Harvester Unit
- Wind Harvester Unit
- Photovoltaic (PV) Harvester Unit
- Storage and Power Processing Unit

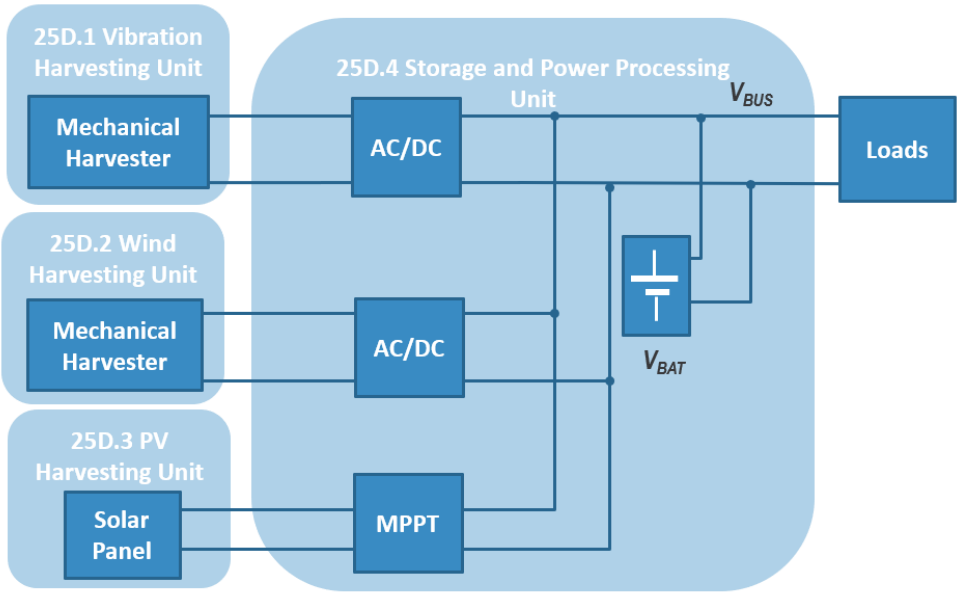

Figure 11: Energy Harvester Architecture

The first component of the Building Block (BB) is named 25D.1 (Vibration Harvesting Unit), and consist of a mechanical device that takes advantage of the rail deflection that occurs when a train passes through the track section where it is installed.

The second component is the Wind Harvesting Unit (25D.2). The idea is to take advantage of the airflow generated in the underfloor area (around the ballast bed) of a passing train. In such case, kinetic airflow energy is high enough for energy harvesting purposes, since the mean induced velocity of the airflow is of the order of 1/3 of the train velocity. That is, for a train at 100 km/h the kinetic energy per unit of time and area would be of the order of 500 W/m2. For operative reasons, the available area between the track and the underfloor is limited, say of the order of 0,25 m x 0,25 m, meaning a source of power of the order of 30 W.

The third component is the PV Harvesting Unit (25D.3) This unit provides the energy that cannot be harvested by the mechanical harvesting units (25D.1 and 25D.2). It is very easy to tailor the unit in order to satisfy the energy requirements for any particular application.

The fourth component is the Storage and Power Processing Unit (25D.4). This unit combines the energy harvested by the multiple sources: Wind harvesting unit, Vibration harvesting unit and PV harvesting unit, and controlling the power flow between the sources, the energy storage device (battery) and the loads.

The main functionality of this component can be summarized as:

1) Control the current drawn by the electrical generators of the mechanical harvesters, components 25D.1 and 25D.2, in such a way to obtain maximum power from these energy sources.
2) Providing maximum power point tracking (MPPT) of the PV panel (component 25D.3)
3) Battery management. Controlling the power flow between the harvesters and the load and keeping the battery state of charge.

The AC/DC converters will interface the electrical generators of the mechanical harvesters controlling the electrical load torque of these generators to operate the harvesters in their maximum harvesting point.

The MPPT converter will control the operating point of the PV so that the maximum power is extracted from this source. In the case that the battery is already charged and the load demand is smaller than the peak power of the PV panel, the MPPT will limit the power extracted to satisfy only the load demand.

The harvester design considering the energy, not the power, as the limiting factor, has been conceived considering two possible scenarios:

1) Scenario 1 (High energy demand). Equipment power consumption is 20W during a day (16 hr) and 1 W in standby during a night (8hr)
2) Scenario 2 (Low energy demand). Equipment power consumption is 10W during 20 s (when the train passes) and 0,1 W in standby (rest of the time)

Regarding the frequency of trains, that it is related to the energy harvested, it is assumed a frequency of 5 trains/hr during the day (16hr). In Table 1, the main variables of the two scenarios are summarised. Pay attention that in Scenario 1 the Demanded Energy per day is 328 Whr, while in Scenario 2 this value is 4.4 Whr, much lower.

Scenario	Demanded Energy per day	25D.1 Energy Generated per day	25.D2 Energy Generated per day	25.D3 Energy generated per day	Battery Capacity
High energy demand	328 W·hr	6.7W·hr	2.2W·hr	500W·hr	10 W·hr·
Low energy demand	4.4Whr	6.7W·hr	2.2W·hr	Not needed	1W·hr

Table 1: Testing scenarios

3.4.1.2 Vibration harvester Unit

The first energy source analyzed for the harvester is the rail vibration/deflection unit. It tries to harvest some energy due to the mechanical energy dissipated by the rail movements induced by the train.

After assessing several options, the power requirement led to a system conceived to extract some energy from the deflection caused in the rail when the train passes through a point of the track. The displacement produced should be converted into a rotational movement by mechanical means. A lever attached to the rail has been used (Figure 12)

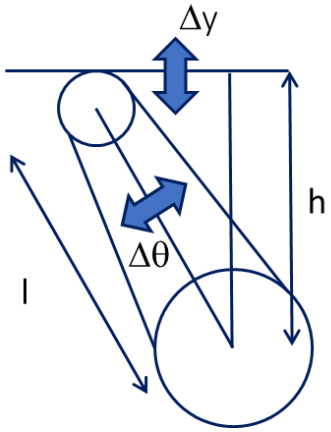

Figure 12: Lever attached to the rail, converting vertical displacement in rotational movement

If $cos\theta = h/l$, the deflection can be calculated as:

$$\Delta\theta = \frac{\Delta y}{lsin\theta}$$

So, the deflection will be greater when the lever is placed near vertically. This effect has been assessed in lab tests varying the deflection of the lever.

The arm attached to the rail is connected to an axis with a freewheel, so when the rail deflection is moving the lever, this action is applied to the axis. When the lever returns to the still position, the freewheel disconnects the lever from the axis.

Several freewheels have been used, because torsional load over it can be very high (with torques up to 1000 Nm). Freewheels of various stiffness have been tested, some of them in Figure 13. The smaller ones have suffered destructive failures due to their resistance was not enough for the application.

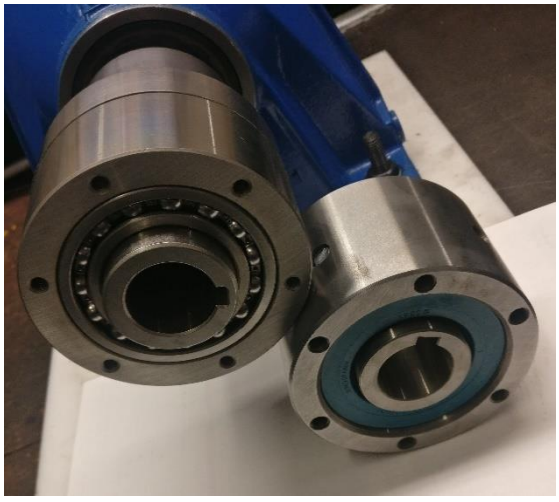

Figure 13: Freewheels with high stiffness

The deflection of the lever, or arm, is amplified by a gearbox with a fixed speeds relationship. 8.63:1 and 20:1 gears have been used.

In the high speed axis, a flywheel stores energy during the impulsion phase, and delivers that mechanical energy during the rest of the cycle.

In the tests performed, various flywheels have been used, with the logical conclusion that the bigger the flywheel, the most stable will be the rotational speed of the system. It accelerates when the lever is deflected and decelerates in the rest of the cycle.

Finally, an electric generator is used to convert mechanical power into electric power. The deceleration of the system is due to the action of this generator, besides the mechanical losses.

Figure 14 shows a scheme of the system, naming all the elements.

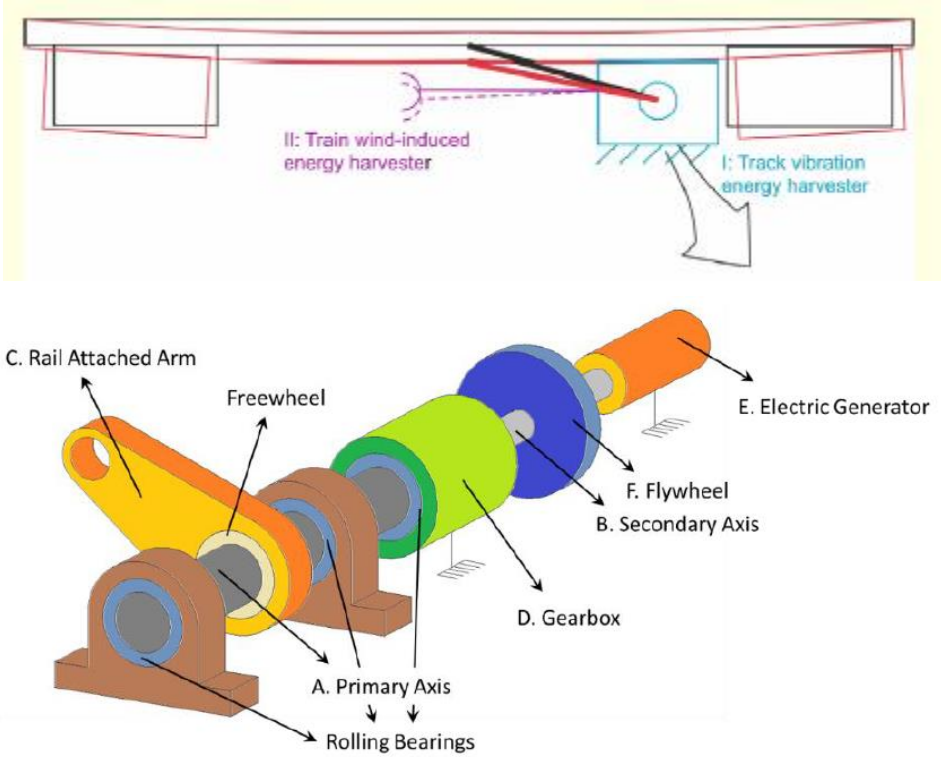

Figure 14: Mechanical Scheme of the harvester

Based on this concept, the work performed can be divided in two separate fields:

- **Mathematical Modelling.** A model has been developed to predict the behaviour of the system, having as results the rotational speed, torque in every coupling and power delivered of energy stored. This model has been correlated with experimental results
- **Experimental Test**. A test rig has been mounted in a modular concept, being able to change some important design parameters as gearbox speeds ratio, inertia of the flywheel, length of the arm, power of the electric generator and resistance of the load.

Figures 15,16 and 17 show different parts of the test bench.

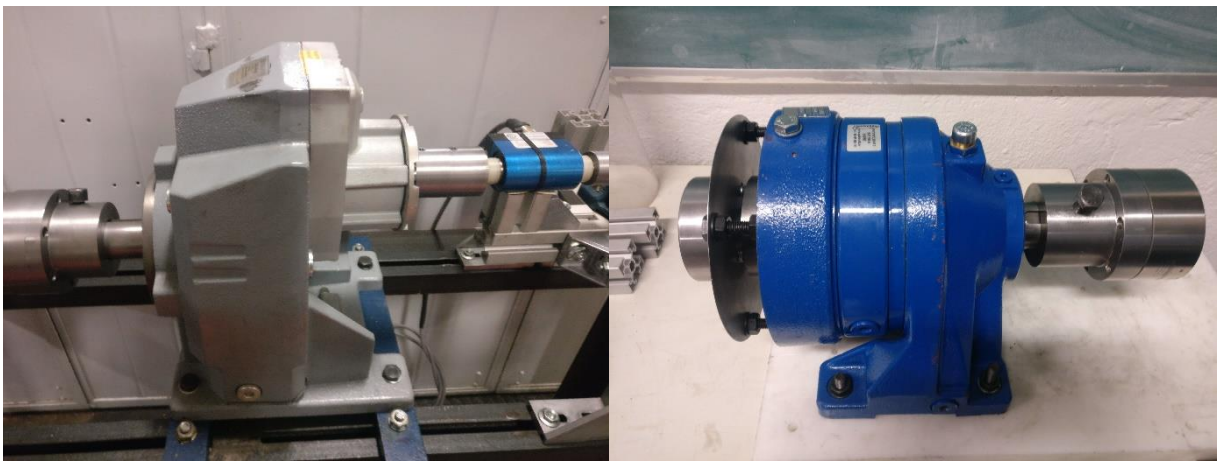

Figure 15: Gearboxes used in the tests

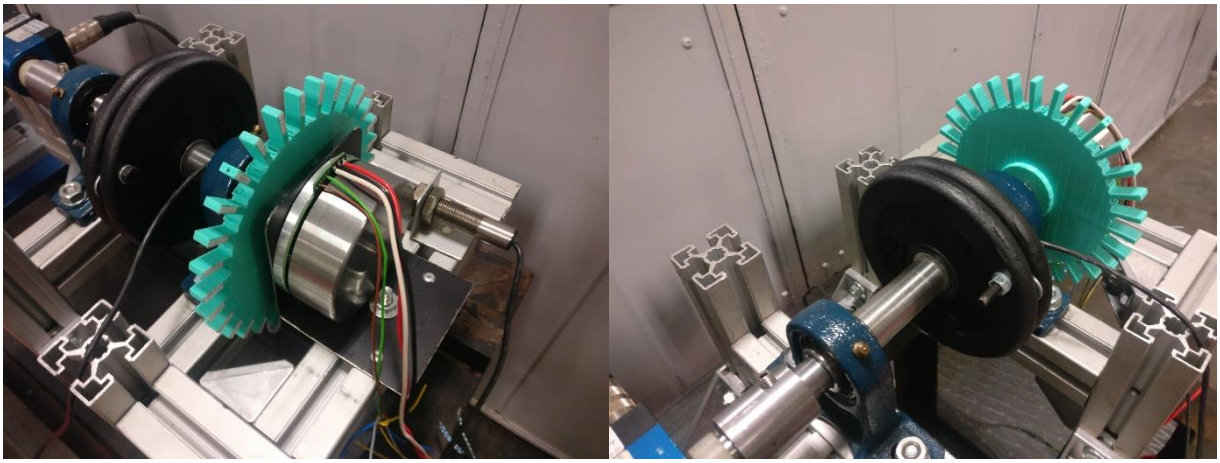

Figure 16: Flywheel (black iron disks) and generator. The green part is a rotational speed sensor

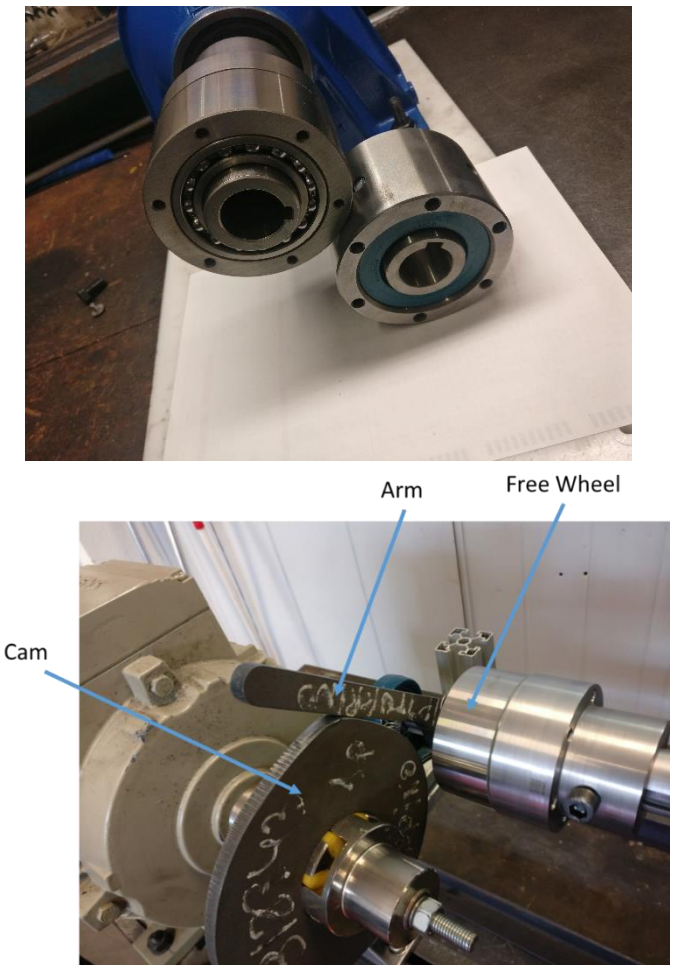

Figure 17: Free wheels and the lever

In the test bench, the rail deflection has been simulated with a rotating cam, in Figure 17.

Two control strategies have been tested in this development:

- Low inertia flywheel. In this case, we have found large variations in the rotational speeds, and the mechanical loads are very low. The system can be reduced in weight and size, but the power delivered is very low.
- High inertia flywheel. Just the opposite to the other case, with lower variations in the speed. In order to maximize the energy stored in every train passing, this strategy is better, increasing the resistance of the load. But very heavy mechanical components should be used.

This trade-off has to be taken into account when the final configuration of the system is to be defined. Location data is needed to make the decision.

A base case can be defined with parameters in Table 2:

Parameter	Value
Cam Height	14 mm
Arm Length	16 cm
Motor Speed	3 Hz
Load Resistance	100 Ω
Inertia of the flywheel	0.025 kg·m^2
Gearbox ratio	1:8.67

Table 2: Base case parameters

In this case, the load resistance is very high, because it is important not to have an electric torque to characterize frictional losses in the system.

With the height of the cam used in this case and the length of the arm, the angle rotated by the arm is:

$$\Delta\theta = arctan\left(\frac{13}{160}\right) = 0{,}081\, rad = 4.6º$$

The angle rotated by the cam during the arm movement is 92º, and with the rotational speed of the motor the average speed of the arm in the lift movement is:

$$\bar{\omega}_1 = \frac{0.081}{\frac{46}{360 \cdot 3}} = 1.9\frac{rad}{s} = 18.18\, rpm$$

And as the movement is harmonic, the peak value is:

$$\omega_{1máx} = \bar{\omega}_1 \frac{\pi}{2} = 28.6\, rpm$$

So, after the gear, the generator medium speed should be 250 rpm.

In Figure 18, we can observe the voltage obtained after the diode bridge in this configuration. There are three pulses, due to the rotational speed of the cam (3 Hz). The curl in the curves, due to the condenser of the diode bridge, is not present anymore once that the electronic control system has been attached to the three-phase output of the generator.

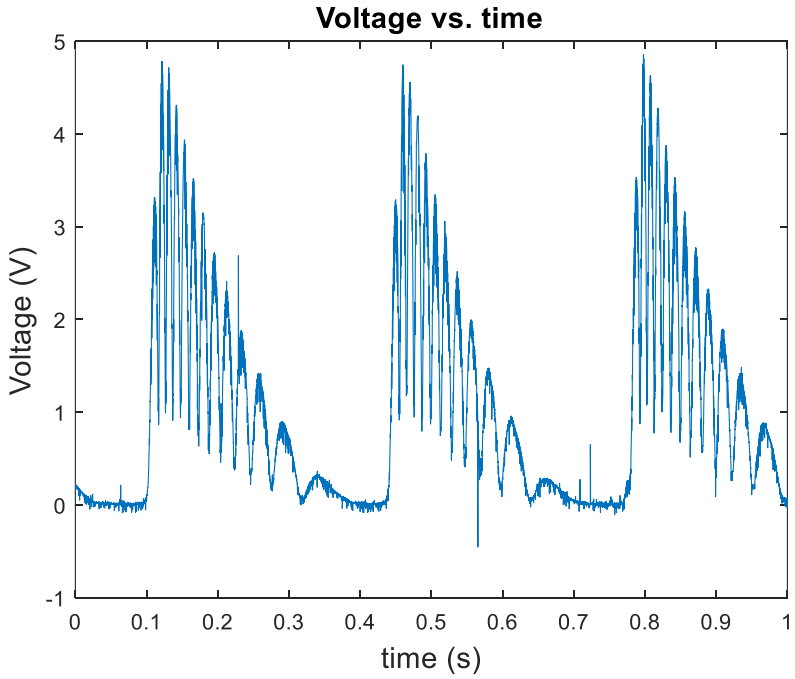

Figure 18: Output Voltage in the Base Case

With a mathematical treatment of the 4096 pulses encoder, the rotational speed can be evaluated. In Figure 19, the signal from the encoder is schematized.

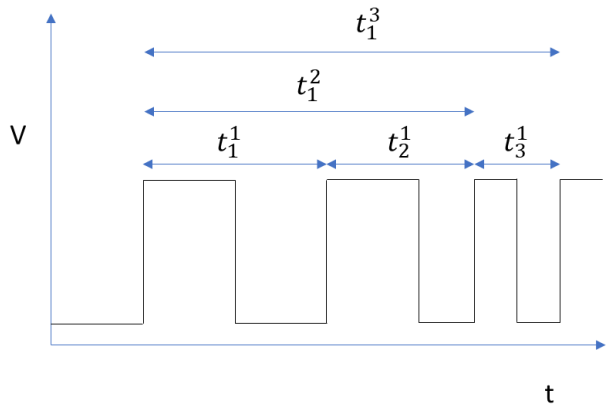

Figure 19: Signal from the encoder

If the time between pulses is evaluated in every pulse, the instantaneous value of the rotational speed would be:

$$\omega_i = \frac{1}{4096 \cdot 2\pi} \cdot \frac{1}{t_i - t_{i-1}} \left(\frac{rad}{s}\right)$$

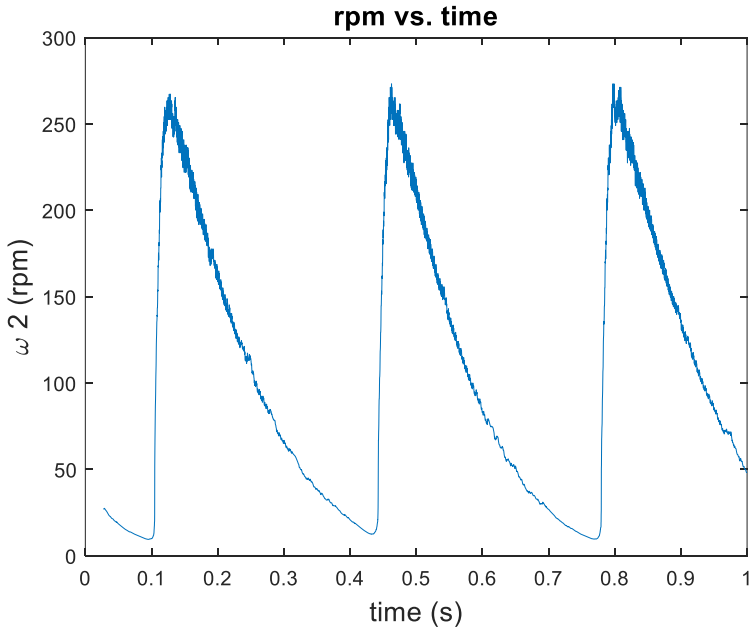

Figure 20: Rotational speed counting time between 50 pulses

The maximum speed in these conditions is about 250 rpm, as was predicted in the first calculations.

Finally, one can see in Figure 20 that the speed decreases very fast from its maximum, even in this case with a high load resistance (100 Ω) where no effective torque is produced. This is due to the frictional torque in the gearbox and in the freewheel (much lower because the torque in the generator side is 10 times higher).

To make an assessment of this friction, it can be assumed that the friction is proportional to the speed, so:

$$T_f = -C \cdot \omega$$

And the equation of movement is:

$$-C \cdot \omega = I \frac{d\omega}{dt}$$

Counting time from t=0, and with an initial condition ω0, the rotational speed has a value of:

$$\omega = \omega_0 e^{-\frac{C}{I}t}$$

Adding a new time reference, Figure 21 shows how the rotational speed decays in time and an exponential curve fitted by minimum squares technique.

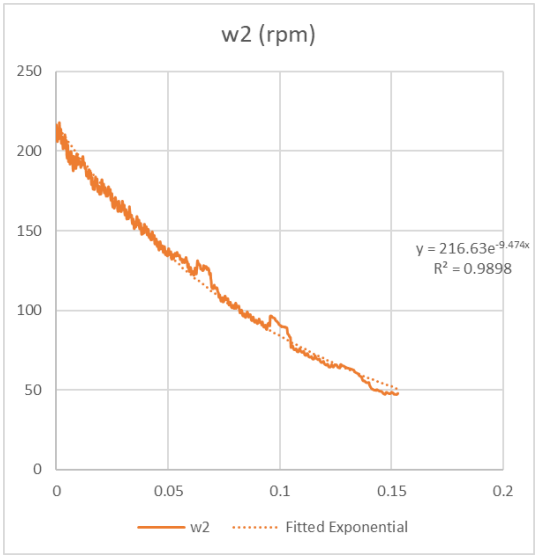

Figure 21: Fitting an exponential curve to the measured speed

The exponent of the curve leads to a relationship between the friction coefficient *C* and the Inertial of the system *I*:

$$\frac{C}{I} = 9.474\ s^{-1}$$

The tested prototype has a flywheel with an approximated inertia of 0.025 kg·m^2, and adding the inertia of the gearbox, total inertia of the system is about 0.04 kg·m^2. This leads to a friction coefficient of:

$$C = 0.38\ \frac{Nm}{rad/s}$$

So a maximum frictional torque of 10 Nm is obtained in the gearbox.

Regarding the acceleration slope, the time needed to reach maximum speed is half the time needed to reach maximum deflection. Figure 22 represents the theoretical diagrams of lifting and rotational speed in the secondary axis, where you can see the difference between the theoretical model estimating the rotational speed and the actual measurements of this variable. The theoretical calculation is quite accurate.

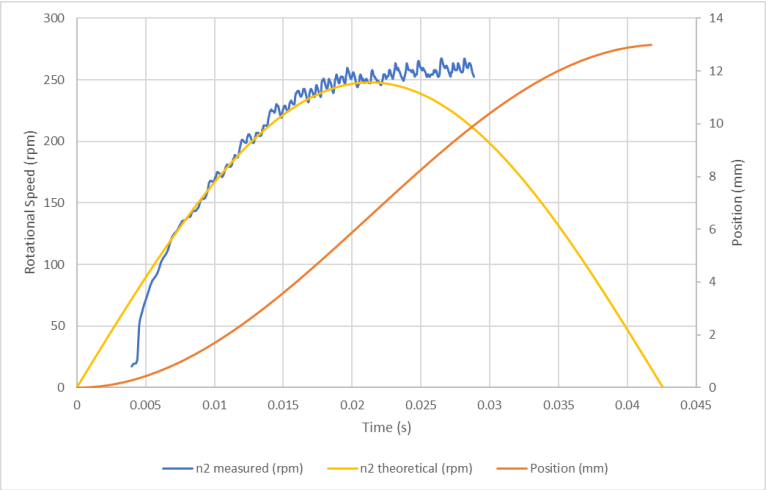

Figure 22: Theoretical vs measured rotational speed

Theoretical values of lift and rotational speeds are given by the expressions:

$$y(mm) = \frac{160}{2}\left(1 - cos\left(2\pi\frac{t}{T}\right)\right)$$

$$\omega = \omega_{max} sin\left(2\pi\frac{t}{T}\right)$$

At the beginning of the movement, there is a considerable slide between theoretical and measured speeds, due to the infinite acceleration needed at that moment. The cam is braked during 5 ms, and when the motor increases the torque (to maintain the commanded speed) recovers the theoretical movement.

The lift movement is T=42.6 ms long, but in the middle, when the speed is maximum, the secondary axis overtakes the primary one and the separation in the freewheel occurs, so the acceleration process lasts 21.3 ms. During this time, the average torque, in the secondary axis, is:

$$T_m = I\frac{\omega_{max} - \omega_{ini}}{\Delta t} = 0.04\frac{(250 - 32)\,\pi/30}{0.0213\ s} = \ 43\ Nm$$

Note that in the slower part, the torque is 373 Nm, a considerable value that requires a very stiff freewheel and resistant gearbox. The peak value of the torque, calculated as the theoretical initial acceleration times the inertia of the system, is 79 Nm. So peak torque in the primary side is up to 685 Nm.

These facts have driven the election of the gearbox and the freewheel, and due to its size, we have such a frictional torque.

Finally, the kinetic energy balance between the initial and the final point gives a work done by the cam:

$$\Delta K = \frac{1}{2}I\left(\omega_{max}^2 - \omega_{ini}^2\right) = 13.5\ J$$

And the average power during 0.0213 s:

$$\dot{W_m} = \frac{13.5}{0.0184} = 634\ w$$

Work dissipated by friction is:

$$W_f = \int_0^{\alpha} C\omega d\alpha = \int_0^{t} C\omega^2 dt = 17\ J$$

This value is higher than the energy stored in the acceleration due to the elastic energy accumulated during the positive torque. The elastic deformation of the axis is returned to the system just when the maximum velocity is reached, and the separation of both axes occurs. A part of these 17 J should be converted into electricity in our system when the resistance load is lower than this case.

Figure 23 presents speed vs time for two different load resistances . This is important to highlight the impact of the electric load value in the system response and the need to optimize the load value to maximize the harvested energy. This is the role of the AC/DC converter in the interface with unit D24.4

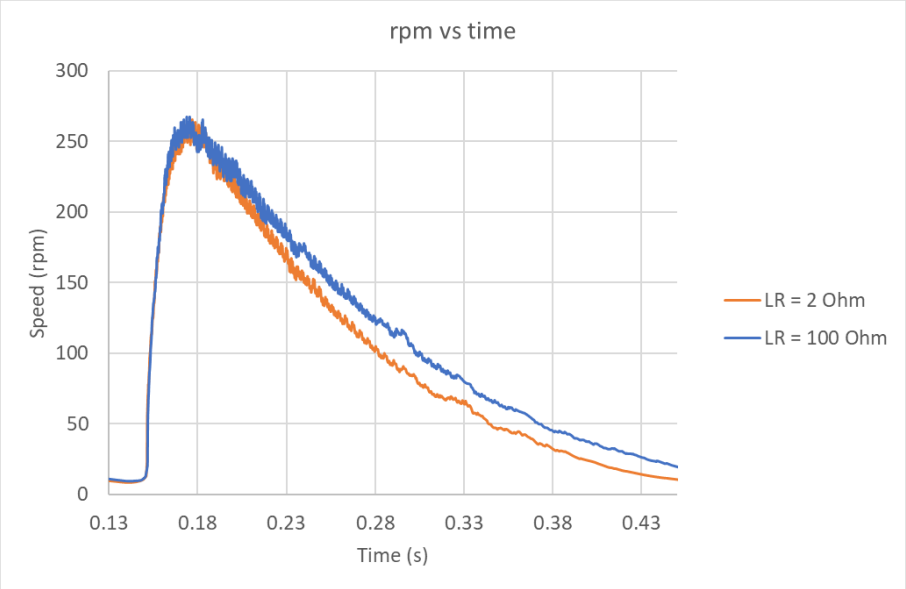

Figure 23: Base case vs 2 Ohm rotational speeds

Summarizing, the following achievements have been reached:

- It has been demonstrated the effectiveness of the system
- A mathematical tool has been developed and can be used to obtain the optimum design for a specific location, taking into account rail deflection (train weight and speed), frequency of trains and the hardness of the ground
- Values up to 5 J per train wheel can be obtained with a proper design.

3.4.1.3 Wind harvester Unit

The idea behind the wind harvester is to take advantage of the available energy in a passing train due to the airflow displaced by the train. The kinetic airflow energy can be high enough for energy harvesting purposes if the speed of the train is significant, since the mean induced velocity of the airflow is of the order of 1/3 of the train velocity.

The wind harvester unit is based on a Savonius turbine, which is a very interesting approach in microgeneration due to its simplicity, low cost, reduced maintenance and low environmental impact. This device is a drag driven vertical axis wind turbine that performs independently of the wind direction, showing a good-self-starting capability. All these characteristics make the Savonius turbine

an excellent candidate for energy harvesting from the wind with high changes, both in magnitude and direction.

The airflow around a Savonius turbine is very complex and to date, there is no analytical theory to find an optimal design. Several questions are still open, for instance, the optimal geometry of the rotor or the role of the influence of airflow speed on the Savonius performance. Several Savonius turbine laboratory prototypes (TRL 4) were built and tested in the wind tunnel in order to find: (i) the best (most efficient) geometry of the rotor and (ii) the functional dependence of the electrical power generated as a function of the incoming airflow speed.

Figure 24 presents a picture of the experimental set-up. In operation (during the test), the fan generates an airflow with fixed speed. The airflow speed is controlled by varying fan speed rotation with a variable frequency driver. Airflow speed was measured with a differential pressure sensor and Pitot tube. The airflow around the Savonius generates an aerodynamic torque and spin motion around its vertical axis, which drives the electrical generator producing electrical power. Electrical power generated was measured with an oscilloscope.

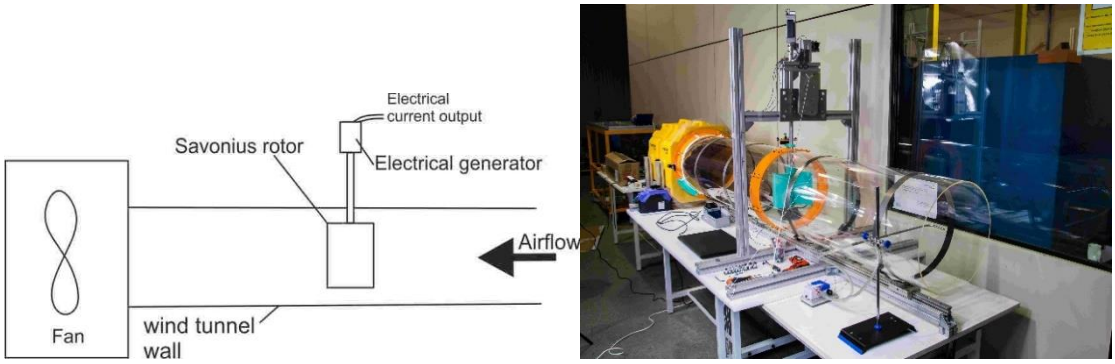

Figure 24: Left: Schematics of the experimental set-up. Right: Picture of the experimental set-up

Looking for the most efficient geometry of the rotor, several tests were carried out with different geometries with a cross-section of 200 mm x 200 mm. Each rotor tested was manufactured using 3D printing in PLA. (Polylactide), see Figure 25.

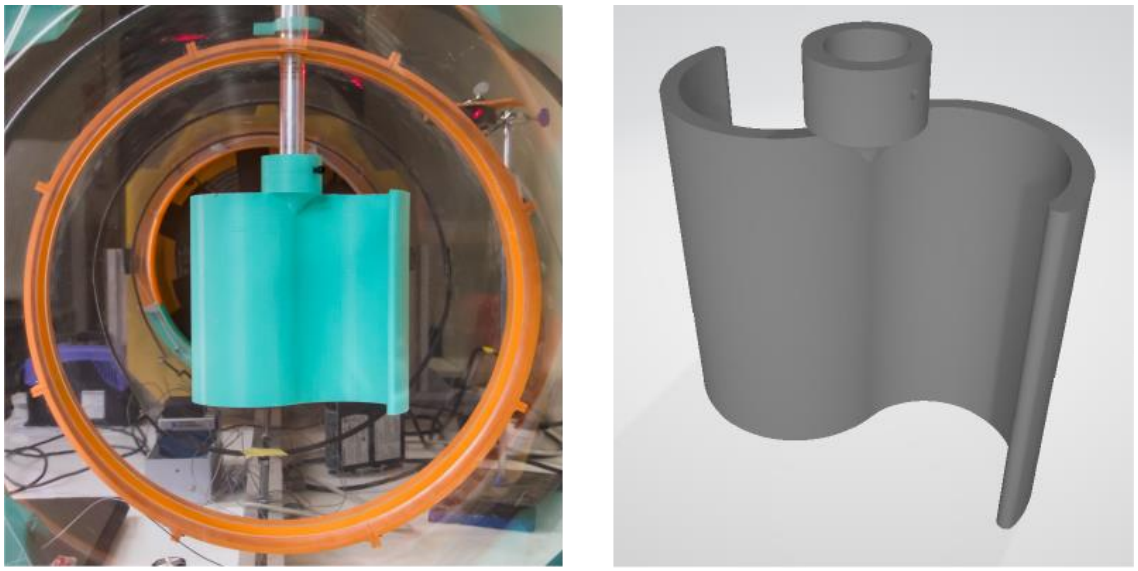

Figure 25: Left: Savonius rotor (two semi-circular blades) in the wind tunnel ready for the test. Right: CAD model of the Savonius rotor (two semi-circular blades).

From laboratory tests, it was found that the most efficient geometry consists in two semi-circular twisted blades, which was considered to manufacture the final Savonius configuration (see Figure 26).

Figure 26: Final design of the Savonius turbine

For the final Savovius design (two semi-circular twisted blades) the relationship between electrical power generated *Pe* (in Watts) and incoming airflow speed *U* (in m/s) was found during the laboratory tests:

$$P_e = 0.019U^3$$

3.4.1.4 PV harvesting unit and integration

Figure 27 shows the current-voltage curve of a panel. A Solar (PV) Cell or a Panel / Module produces its maximum current when there is no resistance in the circuit, i.e. when there is a short circuit between its Positive and Negative terminals. This maximum current is known as the Short Circuit Current and is abbreviated as I_{sc}. When the Cell / Panel (Module) is shorted, the voltage in the circuit is zero. Conversely, the maximum voltage occurs when it operates under NO load conditions. This is called the Open Circuit Voltage (V_{oc}). Under this condition, the resistance is infinitely high and there is no current, since the circuit is incomplete. There is a point on the knee of the I-V Curve where the maximum output power is located and this point is called the Maximum Power Point (MPP). The voltage and current at this Maximum Power Point are designated as V_{mp} and I_{mp}.

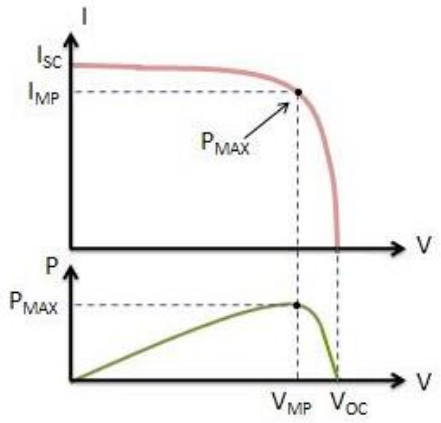

Figure 27: Charging current for the battery

The MPPT charge controller is a DC to DC converter that can transform power from a higher voltage to power at a lower voltage. The amount of power does not change (except for a small loss in the converter process). Therefore, if the output voltage is lower than the input voltage, the output current will be higher than the input current, so that the product P = V x I remains constant. The maximum power collected from the PV panel is about 33W.

3.4.1.5 Storage and Power Processing Unit

The Storage and Power Processing Unit is responsible for the optimal recollection and storage of the energy generated by the three harvester units. It has been optimized to get the maximum efficiency and the final design has been optimized and tested. Figure 28 shows the whole electronic system to store energy. The integration of the three harvester sources has been validated, AC/DC converters for vibration and wind harvester units and the MPPT converter for the solar panel, are controlled to behave like a current source that is injected to the battery independently. This current source behaviour avoids any interaction among the different power sources that inject energy to the battery.

In the experimental validation, having integrated the vibration harvester and the solar panel, the injected power to the battery has been 45W, where 33W are coming from the solar panel, and 12W coming from the vibration unit.

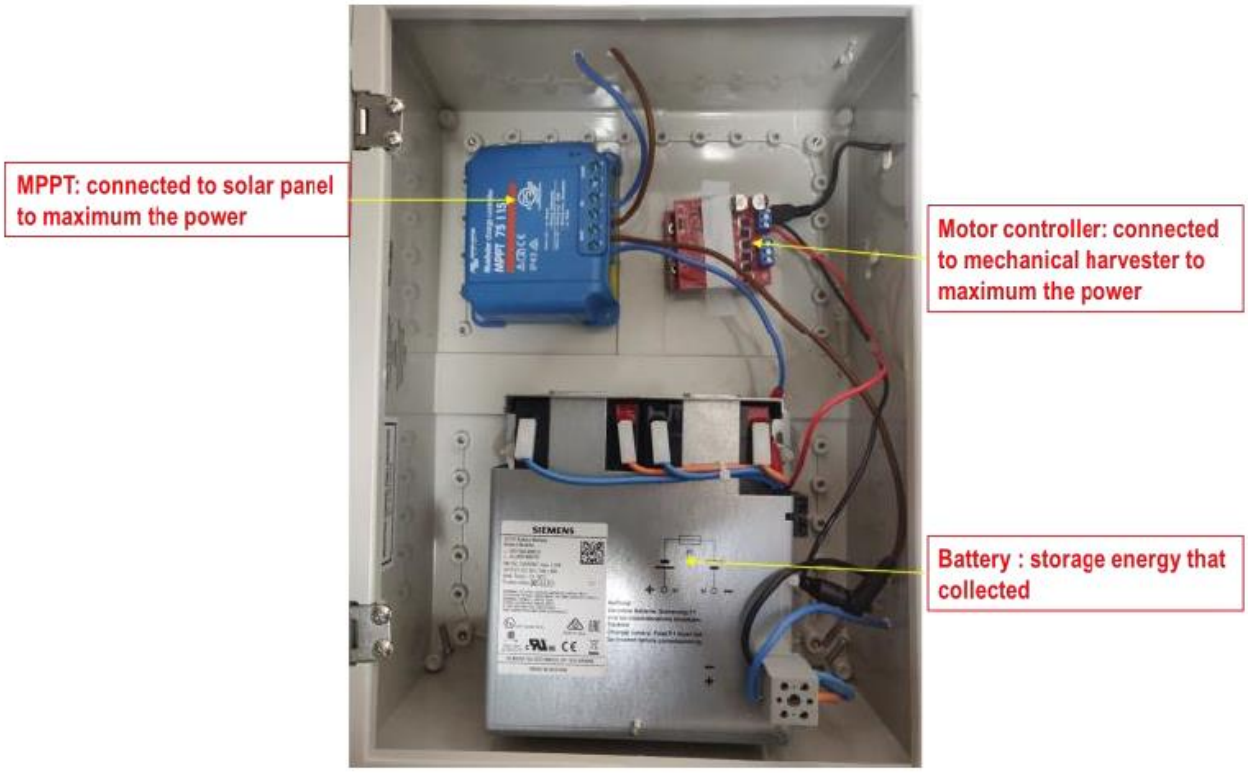

Figure 28: Storage and Power Processing Unit

Each of the mechanical harvesting units (vibration and wind harvesting) is mechanically coupled to a Brushless Direct Current (BLDC) motor/generator, being this motor driven by a three phase AC/DC converter. Figure 29 shows the equivalent electrical circuit of the three-phase star-connected motor and the AC/DC converter that drives the motor/generator and charge the 24V battery.

The AC/DC converter controls the three-phase voltage applied to the generator, controlling the rotation speed of the mechanical axis that is coupled to the vibration or the wind harvester. This way, the energy is transmitted from the vibration or the wind harvester to the mechanical axis of the generator while the rotation speed is controlled by the AC/DC converter keeping the rotation speed close to the nominal values of the machines, allowing for optimum energy transference.

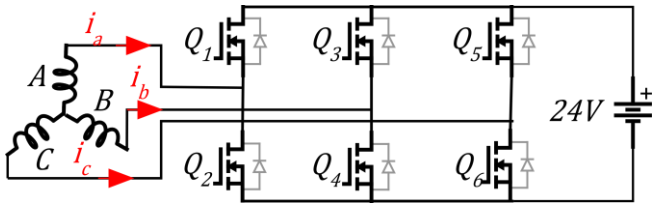

Figure 29: Schematic of the AC-DC power electronic Unit

The three-phase motor will generate three phases of AC current which are 120-degree phase shifted respectively. Table 3 shows the operation sequence, the current direction and the position sensor signals.

Switching interval	Seq. number	Pos. sensors			Switch closed		Phase Current		
		H1	H2	H3			A	B	C
$0° - 60°$	0	1	0	0	Q1	Q4	+	-	off
$60° - 120°$	1	1	1	0	Q1	Q6	+	off	-
$120° - 180°$	2	0	1	0	Q3	Q6	off	+	-
$180° - 240°$	3	0	1	1	Q3	Q2	-	+	off
$240° - 300°$	4	0	0	1	Q5	Q2	-	off	+
$300° - 360°$	5	1	0	1	Q5	Q4	off	-	+

Table 3: Switching sequence

The used control strategy is the Pulse-Width Modulation (PWM) speed control, which is shown in Figure 30. There are two loops in the controller, which are current controller and speed controller respectively. A speed reference (100rpm) is given to be followed by the real speed, then, the speed controller will generate a current reference proportional to the mechanical torque. The current reference is compared with the measured real current to generate an equivalent DC voltage. In order to protect the mechanical harvester system (not to have a rush hit on the system when the train comes), the current reference is limited to have a relatively slow speed change.

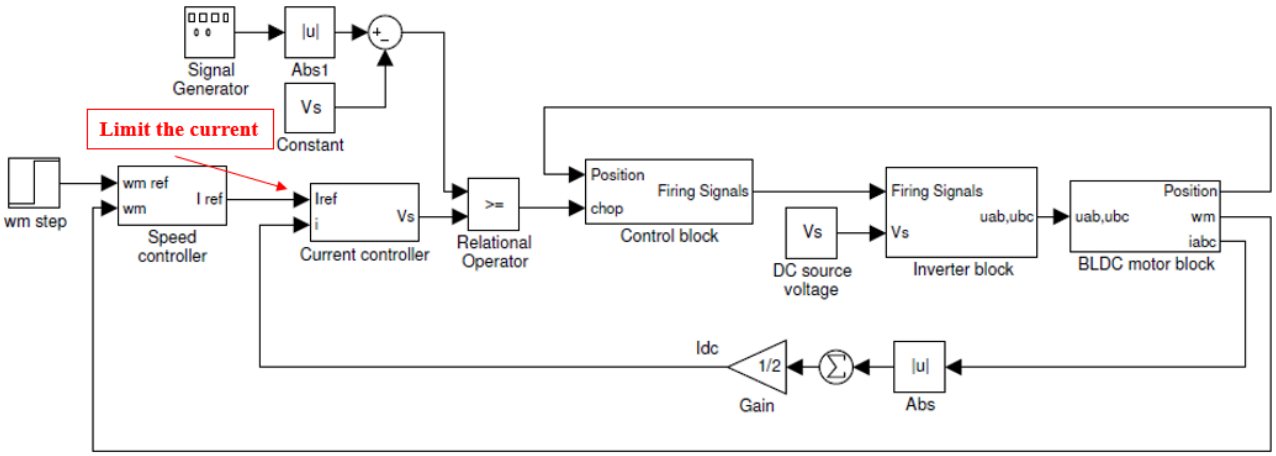

Figure 30: PWM speed control system

Figure 31 shows the estimated speed and torque while, the maximum speed that this motor can reach is 300rpm. By changing current and speed limitation, the maximum speed will change, which will also change the delivered power. Different values are tested to maximize the power that can be collected. In the end, 10W power is collected for a 100rpm speed reference.

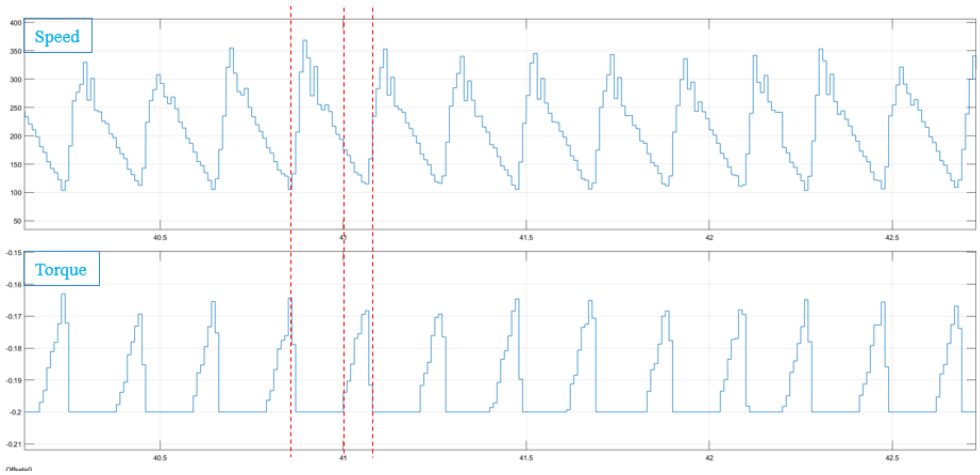

Figure 31: Estimated speed and torque for the motor

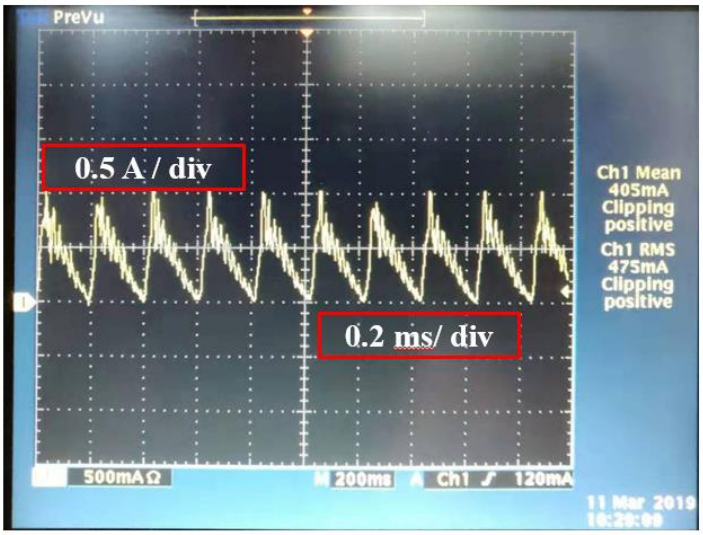

Figure 32: Charging current for the battery

Figure 32 shows the real charging current for the battery (24V), which is observed from the oscilloscope. The average current is 0.5A, and the voltage is 24V. Therefore, the harvested power is 12W, which covers and validates the requirements in scenario 1.

Figures 33 represents the experimental setup in the lab for the unit 24D.1 where the track deformation is simulated by the rotating device located in the left extreme of the picture.

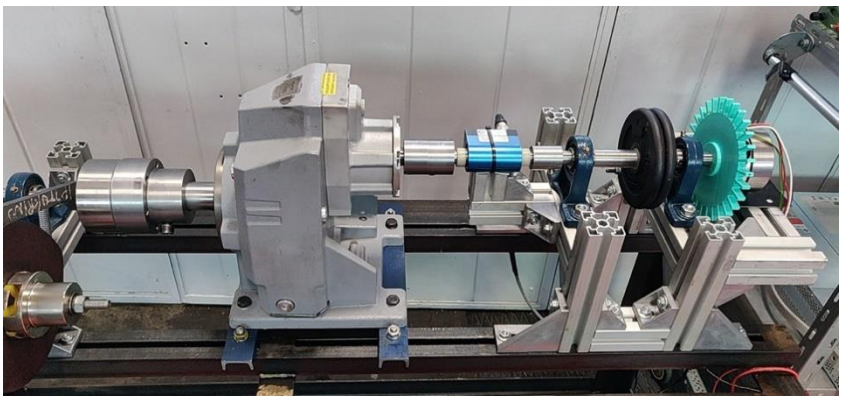

Figure 33: Vibration harvester unit with the DC motor/generator mechanically coupled

3.4.2 Final Status of the Building Block & Contribution to Use Cases

The following list summarizes the status of each of the components of the building block:

Vibration harvester: This part of the system has been tested in different conditions and with different design parameters in the laboratory environment. The mechanical engineering team has tested the system with a constant resistance load, while the electronic engineering team has developed a control system able to optimize energy recovery in very different conditions.

A mathematical model has been also developed, so we have a tool that can be used to design a specific vibration harvester for every location.

On track tests would be important to characterize specifically the rail deflection, so an actual assessment of the energy availability could be performed.

Wind harvester: A prototype of the Savonius wind harvester has been characterized by laboratory tests. This characterization has allowed to link the electrical power produced with the incoming airflow speed. This is useful to properly estimate the expected energy production in different scenarios. For illustration purposes, let us consider the scenario given in Table 1 (section 3.4.1.1). Taking into account the relationship between electrical power and incoming airflow speed, the total energy generated by the harvester (see section 3.4.1.3) per day E_d would be:

$$E_d = P_e T_T = 0.019(U_T / 3)^3 (N_T L_T / U_T) = 0.000704 U_T^2 N_T L_T$$

Where P_e is the electrical power generated by the wind harvester and T_T the time period of passing trains, U_T is the train speed (note that it is considered three times the airflow speed induced by the train), N_T the number of trains per day, and L_T the length of the train. Considering 80 trains per day with a flow speed of 100 k/h (27.8 m/s), and 100 metres of length per train, then it follows that E_d =1.21 Wh, which would be an interesting contribution in scenario of low power demand (see Table 1 in section 3.4.1).

A final design has been manufactured and is ready for further test in a real environment or use case (WP18).

AC/DC converter: a three phase motor/generator is mechanically coupled to the Vibration and the Wind harvester; the motor/generator is driven by a three phase AC/DC converter. A DQ control has been developed and tested to control the rotation speed of the generator, keeping the speed around the nominal values during the energy impulses, optimizing the delivered energy. The developed design and model of the AC/DC converter has been experimentally validated driving the generator coupled to the Vibration harvester and injected the energy in a battery

PV harvester: a Maximum Power Point Tracker (MPPT) converter that makes the PV panel to deliver the maximum power depending on the solar radiation has been designed and experimentally validated.

Energy Sources integration and storage: The three primary sources (vibration, wind and solar) are integrated in a single power processing unit; the AC/DC converters and the MPPT are controlled to behave like current sources that inject the energy in a battery; this concept allows for a complete decoupling operation among the different energy sources.

A final design has been manufactured and is ready for further test in a real environment or use case (WP18). But the contribution to the use case in WP18 is clear in the sense that the harvester is able to supply power to any electronic equipment in the track segment, limited by the available power, conditioned by the traffic in the track and the size of the PV solar panel.

3.5 Building Block BB25.E Improved Energy Harvesting

Wireless sensor networks allow to gather data when the location is variable, and a wired network is not suitable or expensive to be deployed. An ideal wireless sensor would operate indefinitely, with no human maintenance, and collecting energy from different sources where the sensor is located.

This Building Block focuses on gathering energy on environments where 1) the energy source is not predictable or 2) when the source is steady, but it generates few millivolts or even lower (in the range of hundreds of microvolts). This opens a wider set of scenarios, where sensors could transmit data even in places like shady areas or in tunnels with parasitic winds. The low-power prediction algorithm designed previously in BB25.C helps to tune dynamically the rate of transmission, so the sensor data could be retrieved many more times than with standard techniques.

Feedback from real usage in the lab has demonstrated that, using the results of BB25.C for efficient energy management, the resulting low power operating mode for the device allows to use different harvesting methods to collect energy and run indefinitely. For instance, solar cells even at indoor places and low light can provide enough energy in a few minutes to allow the harvester running all day and night without recharging. Other power elements tested can provide energy at low frequency vibrations but the required energy income rate must offset supercapacitor leakage, step up circuitry and microcontroller periodic wakeups to test energy conditions and operation commitments (the device must transmit data from time to time). As a reference, a list of potentially applicable harvesting technologies, as well as harvestable power main figures for some of these technologies are provided below.

Harvesting technologies:

- Solar (or light power)
- Triboelectric effect
- Thermoelectric (Seebeck)
- Coil and magnet vibration
- Wind
- Piezoelectric vibrators or cantilevers
- MEMS

Harvestable power main figures:

- Solar in outdoor: 100 mW/cm2
- Wind at 4.47 m/s speed: 10.4 mW/cm3
- Thermal at ΔT = 5 °C: 60 µW/cm2
- Water drop with size of 0.35 mL at 3.43 m/s speed: 30.67 µW/cm2

3.5.1 Main Achievements of the Building Block

3.5.1.1 Measuring Microvoltages

Ambient sources can vary from high power solar, wind, thermoelectric to low power vibration, wind drafts, static charges or electromagnetic sources. One of the aims in the sub-building block is to investigate and achieve in a real world scenario a harvester capable of getting energy from very low voltage energy sources and multiply the voltage to allow the device to collect data from a sensor and, if possible, transmit the data to a nearby gateway, even if the period between transmissions may be very large (1 day).

Wind drafts and parasitic winds, electromagnetic waves, small vibrations and small temperature differences are suitable for measuring the voltage provided to check if that voltage can be multiplied and even with small currents, gathered successfully.

In order to measure such low values of voltage, a precision instrumentation amplifier has been selected. In-amps are op-amps with a very good common-mode rejection so small differences between the positive and negative inputs can be perceived. The selected chip for the operation is the INA188. A protoboard has been used to allow plug/unplug resistances depending on the type of energy source and the frequency of the source to achieve optimal results.

By using a high end in-amp the real measured values are more reliable than using standard oscilloscopes. Furthermore, custom reconfiguration of the layout can be done to adapt sensing precision to different inputs.

The schematic below shows how to set the in-amp device to take measurements form different kinds of low power sources (2-pin connector on the left). A virtual ground is generated to allow also measurements for non-alternate power sources (for instance, on thermoelectric generators). The amplified output can be measured by connecting a probe to the 2-pin connector on the right. The R3 component is a variable resistor to tune the amplification depending on the power source.

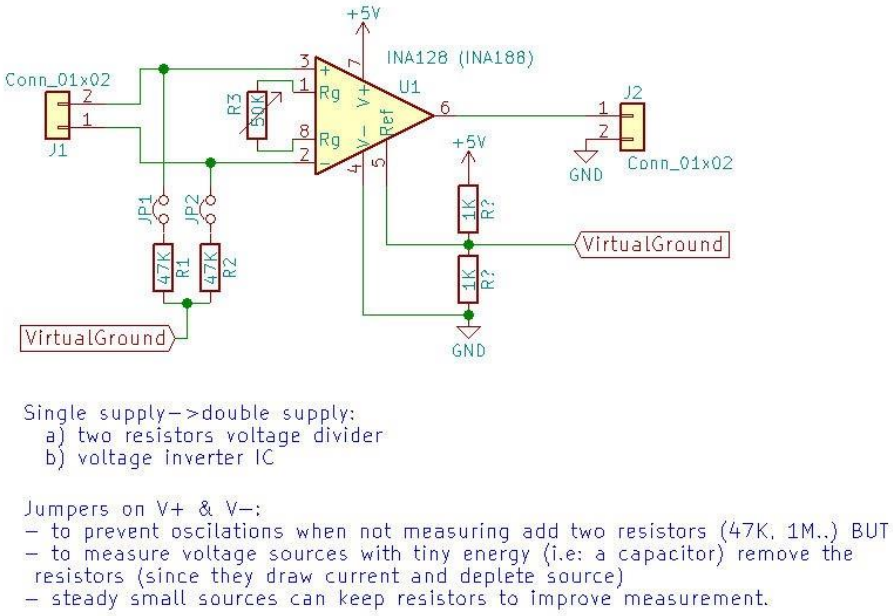

Figure 34: INA188 amplifier

The in-amp output can be later attached to any voltage display. In our case, an Arduino reading the J2-1 pin and displaying data via serial port is enough to check the range of the voltage source plugged to J1 connector. The resistance R3 can vary from no resistance (in this case the gain G=1 to measure ±2.5V voltage sources, R3=5.49Ω for G=10 => ±250mV and R3=511 G=100 =>±25mV).

In the case of G=100, the measure system has 1024 ticks resolution so 50mV/1024=50µV each tick. Higher values of gain (up to G=1000 => tick=5µV) are achieved although not useful since ultra-low small voltages can be measured but not harvested by current technologies.

In order to get real voltage values of a capacitor without depleting the charge in the process, the R1 and R2 should be removed. Measuring capacitors will be interesting in the next steps when elevating voltage from microvolts or few millivolts by using Villard style multipliers. When measuring leakage on normal voltages 1<V<5, a gain of G=1 without resistances R1 R2 is set, and then perform the measures from time to time.

3.5.1.2 Boosting Microvoltages

There are several ways of multiplying input voltage, all of them in field tested and industrialized in specific ICs or components. To multiply alternate voltages a transformer is used. To multiply fixed voltage a boost converter has been included. The problem is that for low input sources these technologies may not be best suited or the performance may be too low.

The first approach is to use a Villard cascade to multiply current, at the same time the current is rectified from alternate current to direct current DC, so the output can be consumed by the board directly (or by using a voltage regulator before). The Villard cascade can be also referred as the Greinacher circuit or the Cockcroft–Walton. The picture below shows a 4X multiplier, the input is 5V AC while the output is slightly lower than 5x4=20V of DC current.

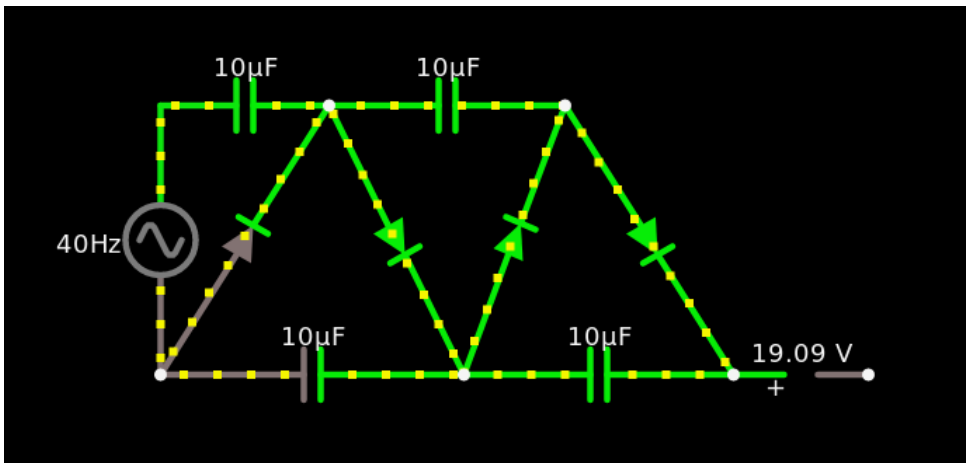

Figure 35: Villard cascade

3.5.1.3 Selecting the microcontroller

Nowadays there are a lot of choices when selecting the best MCU for a given task. There are many microcontrollers with affordable prices and with continuous/stable production while the latest microcontrollers are manufactured with the newest architectures and larger built-in resources. The low-end micros are typically 8 bits MCU with small SRAM and storage. The advantage is that most of them have been proven for years, and the production is done at massive scale, so the availability and the price of these devices are interesting when the tasks to be performed by these micros are not very complex.

On the other side, the ARM architectures are improving at a fast pace for 32 bits, multi-purpose microcontrollers. The efficiency on using resources, the increase in built-in add-ons like bigger storage, memory and program size, and other features for low power consumption or security add-ons allow hardware developers to focus on what are the microcontroller features to simplify the bill of materials required to manufacture the board. Those high-end microcontrollers have also capabilities near to microprocessors, and some technologies are intended to use even an operating system to control resources and interrupts so the program must focus only in the custom logic.

Since the device to be designed to harvest energy must match low cost, high availability and low power consumption as key requirements, the steps for selecting the harvesting MCU unit started by using tested elements like AVR 8 bits MCUs with very small resources capabilities, enough power saving values and affordable price. In the end, the choice of the right board and features will be given by the best performer in several cases (low or unpredictable ambient sources, disposability, ratio of sending signal, better energy management, etc.).

For the Microchip AVR attiny85 (and attiny85V), the datasheet value for sleep mode is less than 100uA. We have performed several experimental tests to measure consumption in active mode, with watchdog enabled every 8 seconds and sleep mode with wake-up pin. The measurement device has been an Agilent 34401A multimeter. The microcontroller is up in standalone mode, with no external oscillator, running with the default oscillator and at 5V steady voltage or using a 3.7 LiPo battery. The following table shows the results in the lab.

Voltage	MCU mode	Measured current
5 V	Active (no load)	2.4 mA (2400 uA)
5 V	Sleep+watchdog 8s	8 uA (8uA)
3.7 V	**Sleep +watchdog 8S**	**5 uA (5uA)**
3.7 V	**Sleep** (wake with pin A0 to reset)	**78 nA (0.078uA)** **(great variability in different measures 120uA-40uA but always far below uA values)**

Table 4: ATTiny85 power consumption

The current experimental values can be compared to the Gammon blog on electronics related to low power consumption on similar ATTiny85 microcontroller and scenario [5]. Values appear to be similar excepting the bare sleep (with no watchdog) where the values measured by the Agilent are far lower than the measured in the blog tests but they are near the AVR datasheet.

A parallel test to validate measures was to load the LiPo battery and measure voltage before leaving the circuit (battery + MCU in sleep mode for 4 days):

- V_{BATT} (2019/02/01 15:30) = 3.941V
- V_{BATT} (2019/02/05 9:45) = 3.933V

Table 5 compares several MCUs with low power consumption and affordable price (Microchip XLP series, Microchip AVR Low power, Texas MSP430, and STM ultra low power) taken either from datasheet or from vendor tests:

Device	PIC24F16KA	MSP430F2252	ATTINY85V	STM32L0	STM8L
Architecture	16 bits	16 bits	8 bits	32 bits	8 bits
Sleep	20nA	100nA	100nA-	?	300nA
Sleep + watchdog	300nA	300nA	?	?	?
Sleep + RTC	500nA	1400nA	X	670nA	?
Price (1U)	1.96€	1.66€	0.82€	1.35€	0.52€

Table 5: Comparison of several low power MCUs

Sources:

https://www.microchip.com/design-centers/lowpower/products/8-bit-low-power-mcus

https://vimeo.com/204703966

http://ww1.microchip.com/downloads/en/DeviceDoc/Atmel-2586-AVR-8-bit-Microcontroller-ATtiny25-ATtiny45-ATtiny85_Datasheet.pdf

https://www.st.com/en/microcontrollers/stm32-ultra-low-power-mcus.html?querycriteria=productId=SC2157

https://www.farnell.com/

3.5.1.4 Harvester main components

Harvester hardware:

- **Energy harvesting module** or battery: The energy source.
- **MCU**: containing the logic for adapting timeslots and sending signals.
- **Radio unit**: currently the inexpensive 433 modules are used but other modules and technologies can be attached.

Harvester software:

- **433 serial comm**: check id [4..n] based on a rule (details in code). The id can be variable length (typically 4 digits, but any value could be used).
- **Energy prediction algorithm (from Building Block BB25.C)**: based on battery/storage value, adjust the timeslots to emit an alive signal.
- **Energy level measurement**: adapted depending on the storage system. Battery discharge and supercapacitor discharge has very different curves.
- **Sleep modules**: either by using a built-in 8 seconds watchdog timer or by using a wake-up pin.

3.5.1.5 Testing the sleep and watchdog features

This part is useful to set the MCU into sleep mode as much as possible to save energy. The harvester must be dedicated only to gather energy, while keeping all secondary devices stopped. The energy prediction algorithm is executed periodically, and the communications module is only started when energy conditions are good.

There are several options to wake the device from sleep:

- by adding a wake-up pin. The start-up is on-demand from another element. If conditions are met, a change of a pre-set pin in the MCU is enough to start it up. This mode would be the best for energy savings, but it requires external circuitry.
- by adding a watchdog timer: The MCU is started from time to time, in the current MCU every 8 seconds. Then the code takes the decision to execute actions or not and then go to sleep again. In this mode, there is only a controller for all the harvesting device (1 MCU and no comparator or external logic chips).

At this stage of the project, the current configuration is using a watchdog because the energy wasted compared to the other option is still acceptable on low energy harvesting environments, and the cost and complexity of the harvesting device is lower. It shall be noted that cost is a variable as important as energy efficiency ratio for these devices, because they are intended to be disposable.

3.5.1.6 Testing the battery level

The battery level can be measured using external voltage comparators, but this approach has two main drawbacks:

- a secondary battery is needed to act as fixed voltage, and therefore, required.
- the system must be also set to sleep periodically to save energy consumption.

For these reasons, we have opted to use internal voltage references after waking up the MCU. This solution is not very precise in terms of measuring the real voltage (and battery/supercapacitor charge status) but it uses the internal circuitry, so no added cost of components or complexity, and the energy spent on that extra operation is very small compared to the general operation.

3.5.1.7 Testing the radio communications via 433 radio

The 433MHz inexpensive radios are chosen at this stage because the real range is acceptable (hundreds of meters) and the cost of the radio solution is very cheap compared to other technologies. The main disadvantages are the ratio of failures (to be compensated by software noise reduction) and the security (it must be set for software).

For preliminary tests on Arduino devices, the results were promising, but when adapting the code to the ATTINY85, the chosen library (Radiohead) was not compatible, and the "*Manchester*" library was evaluated, but the field range in real experiments (indoor and outdoor) with the same radio devices was much worse. Therefore, another library was selected (RCSwitch) even if not as useful as "*Radiohead*" because of sending numbers only (instead of custom variable-length alphanumeric) and a little lower range.

Regarding the hardware for experiments, the most inexpensive commercial radios were bought and some of them adapted (while being still compliant with EU regulations) to allow better default range at lower voltages.

Main highlights:

- Radiohead for receiver does not work on ATTiny. Anyway, this solution could also be chosen because the receiver (in the scope of the project) can be a non-power-efficient device (and it could be an Arduino Nano instead of the tiny).
- Manchester library was very problematic on the effective range when using the attiny85.
- RCSwitch library has enough compatibility (devices), features (at least, sending IDs) and range (less than Radiohead but still acceptable) to be chosen. This library allows the receiver to be installed into the same MCU selected for the harvester and the total size of the receiver will be small compared to the receiver antenna.

Estimated production cost of the integrated solution for the harvesting device: €5. Maintenance: none. Installation: stick and forget.

3.5.2 Final Status of the Building Block & Contribution to Use Cases

Status

Completed. The cost, availability of parts, range, and consumption parameters have been achieved successfully. Different energy sources have been evaluated on the same harvester engine. Since the device is intended to work on the WP17 use case, the energy intake part will be either a solar

cell (this option is capable to fully load the harvester even in indoor light conditions and the harvester can run all night with that stored energy) and a piezoelectric cantilever device to allow charging and operating on movement (low frequencies) events. This will allow using the supercapacitor option as storage (see BB25.C). The supercapacitor not only beats the LiPo battery in charging speed, but also the electronics required for charging the storage can be deleted from the harvester design, making it simpler and cheaper.

Contribution to Use Cases

The harvester device designed in this building block will serve as a secondary positioning system for train wagons and containers deployed in the WP17 "*Safe freight and traffic management in intermodal logistic hubs*" use case. The main positioning system will be performed by GPS devices located carefully and statically in the wagons, so they can communicate with the train central gateway, and therefore, to the freight management system. These devices can provide good location precision and other useful values as speed, but the downside is the battery consumption. In some cases, the batteries could be depleted, and the exact position of the wagon could not be set before planning the train composition.

Here is the aim of the improved energy harvesters, to be developed in the current building block. Since these devices can run autonomously and energy should not be an issue, they can send information about the last known position, and this secondary positioning system should match the main one (sent by GPS devices). If the main device is alive, its position and the harvester position should be similar. If the main device is off, the harvester is providing the area where the wagon or container is located. If both devices are on, but location differs, the train planning operator might check manually if the wagon is where planned, otherwise the train could leave the train station with different wagons (and therefore different commodities or loads) than the planned.

The trade-off for the harvester is the low precision (it is related to areas, i.e.: precision = ±25meters) and the time where the last signal was sent (10 minutes is OK to accept that the wagon is still in that area, 2 hours could not be enough), but the main advantage is that once the harvester is deployed, no maintenance is required, and since the harvester is designed to be low cost, it can be disposable, so the total cost of deploying this secondary-backup method of positioning is very low compared to the benefit of alerting that a train composition that is about to leave the train station with planned loads could be wrong (and the cost of re-planning trucks and deliveries is minimized).

3.6 Building Block BB25.F In-Vehicle WSN

The goal of BB25.F "In-Vehicle WSN" is a concept study of security aspects in WSN applied in vehicles. In-vehicle Wireless Sensor Networks (WSNs) are necessary to allow measurement of vehicle parameters during tests while driving. The main aspect will be the power consumption of the single sensor nodes because inside the vehicle there is no wired infrastructure to connect the sensor. The wireless sensor nodes are powered by batteries or energy harvesting systems or a combination of both. Thus, the concept considers the energy aspect regarding the operability of the wireless sensor nodes. Furthermore, the concept focuses also on usability and communication security.

3.6.1 Main Achievements of the Building Block

The building block 25.F is split into four concept components that are "sensor node assignment concept", "secure communication concept", "energy efficiency concept" and "online security check concept" as shown in the table below and are described in the following subsections.

ID	NAME OF THE COMPONENT
1	Sensor node assignment concept
2	Secure communication concept
3	Energy efficiency concept
4	Online security check concept

Table 6: Components of building block 25.F

3.6.1.1 Sensor node assignment concept

This concept is based on the Out-of-Band (OoB) communication developed in BB23.F. The sensor nodes are semi-automatically assigned to a network by pairing them with the so called key-box. The OoB communication is based on NFC. The NFC-enabled sensor nodes are placed on the key-box and they exchange the network and the node identification. Furthermore, they exchange the security keys for encryption and decryption.

3.6.1.2 Secure communication concept

The secure communication concept secures wireless communication as well as the supply chain of wireless sensor networks and solves the following problems/questions:

- Is the right software flashed on the embedded devices?
- Is it modified maliciously by a third party during transport or operation?
- Is the transmitted data really from the specific wireless sensor node?
- Is the data modified during wireless communication?
- Hiding information from third parties.

The encryption of the wireless communication is based on the AES cryptography supported by the ultra-low power communication SoCs (nRF52832 from nordic). The communication between the base station, also called Wireless Network Processor (WNP) and the sensor nodes is encrypted using the key exchanged as described in the sensor node assignment concept. Furthermore, the secure communication concept includes a concept to secure the executed software at the wireless sensor nodes. It brings a root-of-trust into the overall system starting already at the production by certifying the components by a trusted certification authority.

3.6.1.3 Energy efficiency concept

The energy efficiency concept targets an energy efficient implementation of both previously described concept parts. The sensor node assignment concept uses NFC which is energy neutral for the sensor nodes in terms of communication demand. The short calculations necessary by the microcontroller were implemented also in an energy efficient way. The secure communication concept uses hardware-accelerated cryptography which is also energy efficient by default. Thus we achieved an ultra-low power design and implementation using ultra-low power functionalities.

3.6.1.4 Online security check concept

The online security concept contains the permanent check of the connection of the physical sensor. This is done at each measurement with very low additional computational demand. Furthermore, the RF communication is continuously analysed regarding conspicuous events. All of this is aggregated into the trustworthiness indicator providing an easy understandable overall view on the system's trustworthiness.

3.6.2 Final Status of the Building Block & Contribution to Use Cases

The final status of the building block is that the four concept components "sensor node assignment concept", "secure communication concept", "energy efficiency concept" and "online security check concept" have been developed. The key findings of the concept with special focus on the "secure communication concept" are submitted to the WFCS 2020 as a conference paper [6]. The overall concept is ready for integration into the UC of WP12. Some parts have been implemented for the demonstration which are secure key exchange via NFC and encrypted communication.

3.7 Building Block BB25.G System Level Availability

The basic idea of Fault Injection (FI) Techniques is to emulate (is in fact imitate) both hardware and software to better predict the final product quality and reliability. To make models of the hardware, a good representation of the actual hardware is needed. In many cases, emulation can be used to evaluate the software components without the (final version of the) hardware. To create those models, the software requires the following:

- Representation of hardware models in transfer functions, derived from hardware simulation tools, physics of failure knowledge, Design of Experiments (DoE), or by using the transfer function from previous hardware versions.
- Models for functional parts of the hardware, to be able to test specific parts only.
- Descriptions of interactions between models (dependency/relation).

In SCOTT PhLi has investigated to what level fault injection can contribute to a fast release of large and complex systems. The approach by itself is quite straightforward and it is indicated in the figure below. Where traditional stress testing adds elevated loadings to the system or product, under fault injection methods the system is tested under the conditions of having a (minor) fault inside. How the system reacts under such a condition can give information on its availability under normal use.

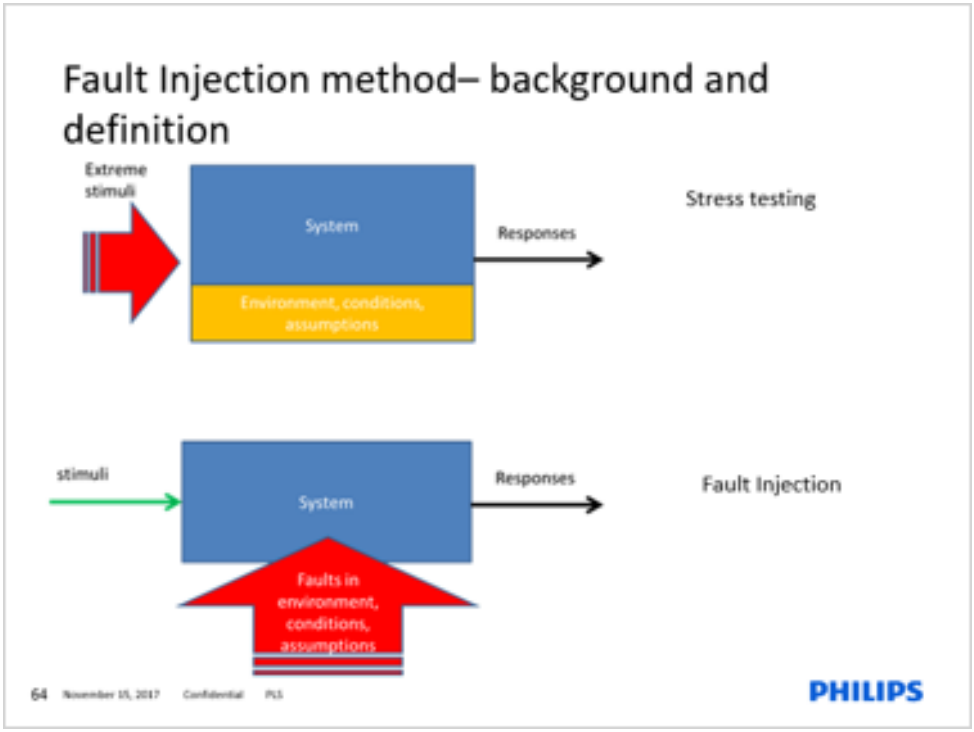

Figure 36: Approach of fault injection; traditional stress testing (top), faults injection (bottom).

The system to demonstrate the technique was a connected office or interact office. InterAct Office provides a complete LED retrofit system and up to 70% energy savings, without upfront capital investment. Hassle-free installation leverages the existing lighting infrastructure, while easy operation saves time and provides peace of mind. You gain crucial insights into your lighting's energy consumption and occupancy patterns across your portfolio. These insights, supported by data, allow you to make decisions on portfolio optimization and bring stakeholders on board with facts. InterAct Office is scaled across all properties in your real estate portfolio, and grows with your needs, enabling unlimited expansion of connected sites and data management. As it uses cloud technology, InterAct Office's intuitive cloud-based analytics dashboard is accessible anytime, anywhere to provide detailed, real-time real estate energy use information. A test bed is available for the investigations, see Figure below.

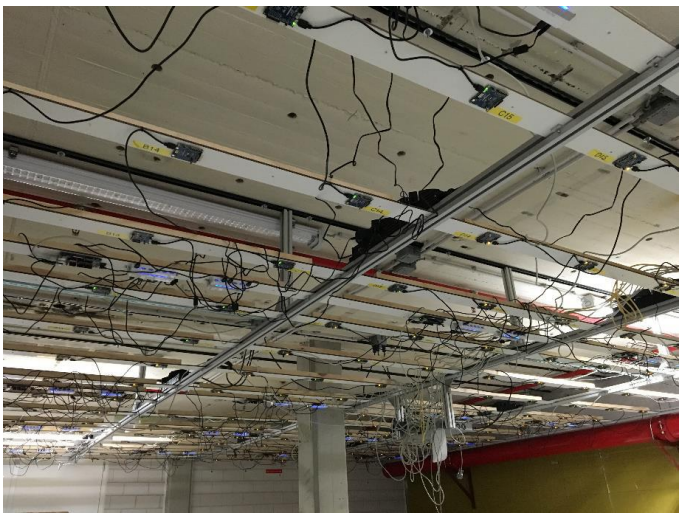

Figure 37: Test bed connected office lighting

The testing approach is listed in the figure below. A reference test is compared towards the test with the fault injection in order to check the system recovery under the worsened conditions.

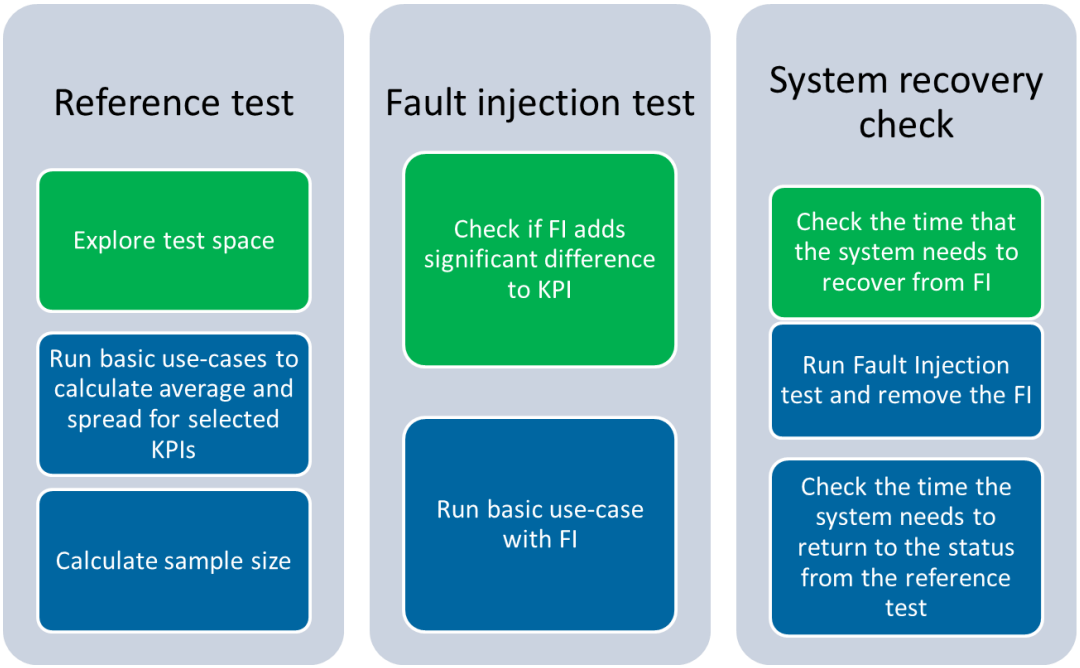

Figure 38: Test description – proposed FI test strategy.

3.7.1 Main Achievements of the Building Block

Main achievements are listed as:

- Testbed is up and running.
  - SPLUNK is used as analyser and all test data is logged into traffic data
- Fault injection is performed, nodes in the corridors are silenced
- We have set-up minimum efforts for application level fault injection, recoverability and fault tolerant scenarios, these are applicable for UCs:
  - Ubiquitous Testing of Automotive Systems
  - Air Quality Monitoring for healthy indoor environments
- Fault injection techniques has become a vital part for the release of the PhLi connected product portfolio.
- Fault injection will enable us to faster release complex systems w/o hampering the quality levels.

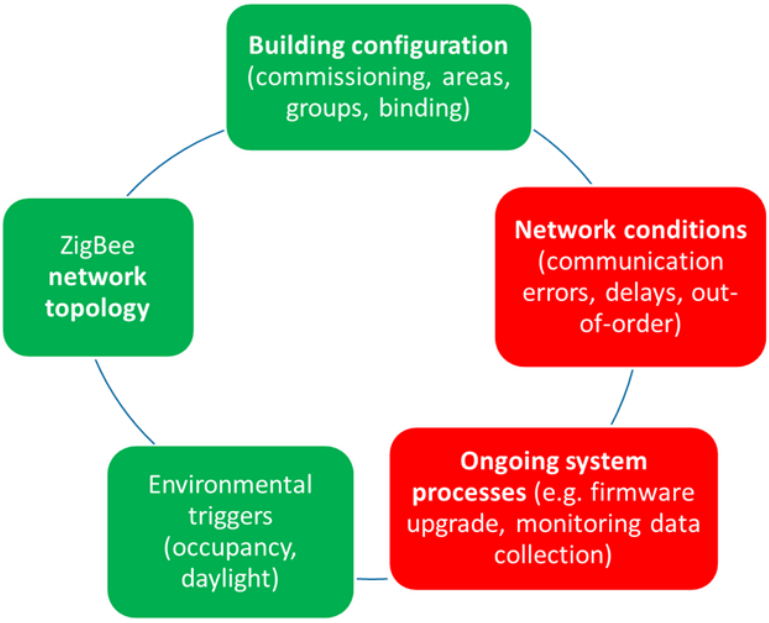

Figure 39: FI test strategy for complex lighting systems.

3.7.2 Final Status of the Building Block & Contribution to Use Cases

The BB technique is contributing to the use case *Ubiquitous Testing*. Other use cases originally also were in scope, e.g. *air quality monitoring for healty indoor environments* and *trustable wireless in-vehicle communication network*. As the fault injection technique is quite general for any complex system, other use cases in the project may also benefit from this work. For that reason PhLi has made connections to the standardisation bodies.

3.8 Building Block BB25.H Dependable and resource-optimised wireless technologies for trustworthy WSNs

The work in this BB25.H “Energy-efficient & resource-optimised concepts for dependable and trustworthy WSNs” covers aspects of energy efficiency and resource optimization, focusing on technologies for the layers above the physical layer, supporting efficient and secure network deployment, runtime operation, and maintenance of in-vehicle networks. This BB is furthermore developing methods to coordinate the interaction between multiple DEWI bubbles. More information about the specific objectives of the Building Block can be found in deliverable D25.2 "*Autonomy of devices / energy efficiency of WSN building blocks – Iteration 2*" [7].

3.8.1 Main Achievements of the Building Block

The BB25.H “energy-efficient & resource-optimised concepts for dependable and trustworthy WSNs” set out to provide inference management for in-vehicle wireless networks based on the IEEE 802.15.4 Time Slotted Channel Hopping (TSCH) technology. We have developed an optimal way of doing robust frequency/channel allocation in an online fashion. This BB has furthermore developed methods to coordinate the interaction between multiple in-vehicle wireless networks, by developing methods to synchronize these networks and concepts for merging them.

3.8.2 Final Status of the Building Block & Contribution to Use Cases

The status of the described elements of BB25.H “energy-efficient & resource-optimised concepts for dependable and trustworthy WSNs” are as follows:

- Provided support for the OpenMote-B wireless sensor nodes in the new release of the Contiki-NG OS: https://github.com/contiki-ng/contiki-ng/releases/tag/release%2Fv4.4
- Implemented and verified our on-line updating of channel hopping sequence changes for IEEE 802.15.4 TSCH in Contiki and OpenMote-B systems.
- Implemented our optimal channel allocation algorithm and compare it to two ad-hoc methods (blacklisting and water-filling) in real-world scenarios.
- Presented a new multi-bubble interference management concept.
- First implementation and experiments of our multi-bubble synchronization concept running on our OpenMote-B systems

4 DISSEMINATION, EXPLOITATION AND STANDARDISATION

Activities related to BB25.A:

Results have been published in [2] and [8]. In addition, the following workshop and special sessions have been organized:

"Workshop on Secure and Trustable Wirelessly Connected Industrial IoT" at the 24th Annual Conference of the IEEE Industrial Electronics Society (ETFA2019), Sept. 10th, 2019, Spain, Zaragoza, Web: http://www.etfa2019.org

Special Session: "Trustworthiness and Security Focused Wireless Industrial IoT Networks" at the IEEE Conference on Factory Communication Systems (WFCS2020), April 27-29, 2020 Porto, Portugal

Activities related to BB25.B:

NXP is active in promoting UWB technology enabled by the building blocks developed in BB25.B and is active in standardization and consortia to develop an UWB eco-system. Some examples:

- Contribution to IEEE 802.15.4z standard https://mentor.ieee.org/802.15/documents?is_dcn=nxp&is_group=004z
- FiRa consortium sponsor member to promote UWB https://www.firaconsortium.org/
- Dedicated NXP internet page for UWB technology https://www.nxp.com/applications/solutions/enabling-technologies/ultra-wideband-uwb:UWB
- Digital Key Release 3.0 is being specified in CCC based on Bluetooth Low Energy (BLE) in combination with Ultra-Wideband (UWB) to enable passive keyless access and to allow secure and accurate positioning: https://carconnectivity.org/press-release/car-connectivity-consortium-unveils-new-features-for-digital-key-specification/

NXP has announced the NCJ29D5 the first of a new generation of automotive UWB IC's that leverage the results achieved by NXP within the SCOTT project:

- https://media.nxp.com/news-releases/news-release-details/nxp-announces-new-automotive-ultra-wideband-chip-capable-turning/

Activities related to BB25.C:

See BB25.E

Activities related to BB25.D:

At this moment, papers in technical journals and conferences have not been produced, assessing the possibility of application for patents, but finally, UPM will not submit any patent from the results developed in the project. Consequently, at this moment several papers are in preparation and they will be submitted shortly.

Besides the consideration about patents, already discussed in the dissemination section, no exploitation activities are already envisaged.

No specific standards are required in this building block. No action regarding standardisation has been taken.

Activities related to BB25.E:

Exploitation

The harvester will be used by TECNALIA for further research and energy optimization. The device will be also installed in the laboratories at TECNALIA for demonstration of ultra-low power connected IoT devices, autonomous non-maintenance devices and power harvesting for feeding other IoT devices.

Activities related to BB25.F:

Results have been summarized in the conference paper “Lifetime Security Concept for Industrial Wireless Sensor Networks” which is submitted to the “16th IEEE International Conference on Factory Communication Systems (WFCS 2020). Furthermore, a special session is co-organized: Special Session: “Trustworthiness and Security Focused Wireless Industrial IoT Networks” at the IEEE Conference on Factory Communication Systems (WFCS2020), April 27-29, 2020 Porto, Portugal.

Activities related to BB25.G:

From the view of dissemination, exploitation and standardisation, PhLi has:

- Written a third internal newsletter in order to broadcast our participation.
- Further implemented the fault injection techniques to become a vital part for the release of the connected product portfolio.
- Gave a keynote presentation on Health monitoring for lighting applications during the Eindhoven Seminar on Reliability.
- Published a book chapter.
- Been active in building standards.
- Connected to standardization efforts for fault injection in the automotive industry.

Activities related to BB25.H:

We have been participating in the organization of a “SCOTT topic” workshop at a flagship conference on factory automation (ETFA):

- “Workshop on Secure and Trustable Wirelessly Connected Industrial IoT”, at the 24th IEEE Conference on Emerging Technologies and Factory Automation (ETFA2019), Zaragoza, Spain, September 10-13, 2019.

We are also planning two additional “SCOTT” workshops at the following international conferences:

- 16th IEEE International Conference on Factory Communication Systems (WFCS), Porto, Portugal, 27-29 April, 2020.
- The 6th annual IEEE MTT-S International Conference on Microwaves for Intelligent Mobility (ICMIM), Linz, Austria, 20-21 April, 2020.

In addition we have published the following paper describing some of the key findings from our work in BB25.H:

> Tomas Nordström and Kristina Kunert, “On the Interference Management Between Non-Stationary Wireless Networks”, Proceedings of the 24th IEEE Conference on Emerging Technologies and Factory Automation (ETFA2019), Zaragoza, Spain, September 10-13, 2019.

Tomas Nordström and Kristina Kunert, “Extended Abstract: Robust Wireless Sensor Networks Based on IEEE 802.15.4e TSCH”, Eighth Nordic Workshop on System and Network Optimization for Wireless (SNOW2017), Riksgränsen, Sweden, 2-4 May, 2017.

The main exploitation, besides supporting WP13 demonstrations, will be using the results as a building block for RISE’s future research and development within the field of autonomous vehicles and dependable IoT systems.

We have so far not been active in standardization effort in relation to BB25.H. But, as a result of the research conducted in SCOTT and BB25.H, there are two additions to the IEEE 802.15.4 TSCH standard we would like to suggest in order to make on-line update of channel hopping sequences and multi-bubble synchronisation possible and interoperable. Therefore, after the demonstrations at the end of the project, showing the benefits of our suggested concepts, we plan to put forward these additions to the IEEE 802.15.4 standardisation working group.

5 INTEROPERABILITY

BB25.A

The implemented BASEBAL routing algorithm extends the EPHESOS protocol and is bound to use enery efficient cryptography. It will be interoperable with existing developments for EPHESOS protocol using a BLE PHY layer and can be used by all SCOTT Building Blocks relying on EPHESOS. Furthermore, BASEBAL can be used on top of any other MAC protocols adhering to a similar superframe/frame/timing structure. The absolute values for the durations of frames/superframes etc. are adaptable to any application as long as PHY and MAC layers support these values.

BB25.B

Interoperability of the UWB building blocks and system is based on the IEEE 802.15.4z standard and the application is aligned with FiRa consortium and Car Connectivity Consortium. This will ensure a broad UWB ecosystem across mobile, automotive and IoT domains.

Even though BB25.B is used in a quite specific application in SCOTT WP14 (i.e., secure car access solution), UWB technology can be used in a wide range of other applications: when mapped to SCOTT's reference architecture *layered physical entity model* (or bubble concept), UWB is most likely used as a level 0 technology providing both secure communication as well as secure ranging & accurate ranging features.

BB25.C

Arduino library wrapper for the energy prediction algorithm.

Source code in C99, for major compatibility with general purpose microcontrollers.

BB25.D

By nature, the BB25.D can be reused to supply power to electronic equipment located in the track segment in many railway applications. The harvesting unit collects energy from three different primary sources (track deformation, wind and solar radiation) and storing the collected energy in a 24V battery. A system model has been developed to optimize the harvester design according to the particular requirements of the application. In that sense, the harvester is highly interoperable being able to be used in many different applications.

Additionally, the battery voltage can be adapted to the particular needs of the application, reinforcing the flexibility of the proposed design.

BB25.E

The harvester is sending information to gateways acting as SOFIA-SMOOL [9] IoT clients so they can flush data to other elements in SOFIA-SMOOL ecosystems without ad-hoc modifications.

BB25.F

The concept study is designed at a high level which makes it easy to apply it to different applications and use cases. Furthermore, it integrates building block 23.F "Out-of-band security" to improve the overall security level which is based on the standardized NFC interface.

BB25.G

Interoperability is one of the tested items in the fault injection techniques investigated by this building block. It was proven that interoperability can be easily demonstrated by setting the correct faults into the system.

BB25.H

We are using open standards like IEEE 802.25.4 TSCH, open source operating systems like Contiki, and protocols suggested by the project reference architecture like MQTT in order to achieve Interoperability. However, as mentioned under standardisation above, there is a need to augment the IEEE 802.25.4 standard in order to fully implement the suggested online updates of channel usage and the multi-network synchronization.

6 CONCLUSIONS

The SCOTT Technology Line of Autonomy of Devices/Energy Efficiency of WSN has developed 8 Building Blocks aligned with the initial objectives of the TL, which were the identification and development of the most suitable energy-related (i.e. energy harvesting, energy storage, etc.) technologies that can be used in different domains and application contexts, the development of energy-efficient components for WSNs, and the development of technologies and methods for supporting the integration of energy-constrained, but at the same time secure and trustable WSNs.

Building Blocks BB25.C, BB25.D, and BB25.E have contributed mainly to the development and integration of energy harvesting/energy storage technologies. In the case of BB25.C, the energy prediction algorithm developed can be used as a power management system for very low-power, low-resource inexpensive devices. It has been integrated in BB25.E, which provides an implementation of energy harvesting in environments with non-predictabable or with very low-voltage (in the range of millivolts or hundreds of microvolts) energy sources. On the other hand, BB25.D has made further contributions to the development and integration of different energy harvesting technologies from two primary mechanical sources (track deformation and air displacement), and from solar radiation.

Building Block BB25.B is a clear contribution to the TL objective of developing energy-efficient components for WSNs, focusing on the development of integrated circuit building blocks for an IR-UWB communications sub-system to be used for distance bounding in secure car access system solutions.

Lastly, Building Blocks BB25.A, BB25.F, BB25.G, and BB25.H have contributed mainly to the objective of developing technologies and methods for the integration of energy-constrained, secure and trustable WSNs. Both BB25.A and BB25.G has focused on the security enhancement of in-vehicle WSNs for automotive test-beds considering energy constraints. BB25.H has focused on supporting efficient and secure network deployment, runtime operation and maintenance of in-vehicle networks, as well as on methods for multi-bubble synchronization. Lastly, BB25.G has provided insights into the application of fault injection techniques which can be used to support faster release of complex WSN-based systems.

7 REFERENCES

[1] H.-P. Bernhard, A. Springer, A. Berger, P. Priller, “Life Cycle of Wireless Sensor Nodes in Industrial Environments” 13th IEEE International Workshop on Factory Communication Systems, Trondheim (WFCS 2017), Norway, Trondheim, Norway, Seite(n) 1-8, 2017 , DOI: http://dx.doi.org/10.1109/WFCS.2017.799194

[2] H.-P. Bernhard, A. Springer, “Energy Balanced Routing for Latency Minimized Wireless Sensor Networks“, *2018 14th IEEE International Workshop on Factory Communication Systems (WFCS)*, Imperia, Italy, June 2018, doi: 10.1109/WFCS.2018.8402350

[3] SCOTT Deliverable D23.3, "*Security Building Blocks – Iteration 2*", v1.0, 2019-05-07

[4] SCOTT Deliverable D12.1, Use Case Specification "*Ubiquitous Testing of Automating System*", v1.02, 2018-09-24

[5] http://www.gammon.com.au/forum/?id=11488&reply=9#reply9

[6] L.B. Hörmann, C. Kastl, H-P. Bernhard, P.Priller and A. Springer, “Lifetime Security Concept for Industrial Wireless Sensor Networks”, submitted to “16th IEEE International Conference on Factory Communication Systems (WFCS 2020)”, Portugal.

[7] SCOTT Deliverable D25.2, *“Autonomy of devices / energy efficiency of WSN building blocks – Iteration 2*”, v1.0, 2019-03-04

[8] H.-P. Bernhard, A. Springer, “Adaptive Period Estimation For Sparse Point Processes”, *Proc. 2018 IEEE Statistical Signal Processing Workshop (SSP)*, Freiburg i. Breisgau, Germany, 2018, pp. 593-597.doi: 10.1109/SSP.2018.8450856

[9] SMOOL project. https://bitbucket.org/jasonjxm/smool

A. ABBREVIATIONS AND DEFINITIONS

Term	Definition
ADC	Analog to Digital Converter
AES	Advanced Encryption Standard
BASEBAL	Backward Structured Energy Balanced Link
BB	Building Block
BLDC	Brushless Direct Current
BLE	Bluetooth Low Energy
BS	Base Station
CCM	Counter Codebook Mode
DoE	Design of Experiments
GP	General Purpose
GUT	Gdansk Technical University
FI	Fault Injection
HRP	High Rate Pulse
IR-UWB	Impulse Radio Ultra Wide-Band
LO	Local Oscillator
MPP	Maximum Power Point
MPPT	Maximum Power Point Tracker
NFC	Near Field Communication
OoB	Out-of-Band
PER	Packet Error Rate
PHY	Physical Layer
PLL	Phase-Locked Loop
PV	Photovoltaic
PVT	Process Votage Temperature (variability)
PWM	Pulse-Width Modulation
RSSI	Received Signal Strength Indicator
SoC	System on a Chip
STRIDE	Spoofing, Tampering, Repudiation, Information disclosure, Denial of service, Elevation of Privilege
ToF	Time-of-Flight
TSCH	Time Slotted Channel Hopping
Tx	Transmitter
UART	Universal Asynchronous Receiver Transmitter
UUT	Unit Under Test
UWB	Ultra Wide-Band

Term	Definition
VCO	Voltage Controlled Oscillator
Voc	Open Circuit Voltage
WNP	Wireless Network Processor
WP	Work Package
WSN	Wireless Sensor Network